UNIVERSIDAD DE COSTA RICA
SISTEMA DE ESTUDIOS DE POSGRADO

BLACK HOLE BINARIES WITH NATAL KICKS

Tesis sometida a la consideración de la Comisión del Programa de Estudios de Posgrado de Física para optar al grado y título de Maestría Académica en Astrofísica

EDWIN SANTIAGO LEANDRO

Ciudad Universitaria Rodrigo Facio, Costa Rica

2023

Acknowledgements

I would like to thank my parents and sister for all of their love and support. I would like to thank Mónica for being always besides me. I am very grateful for all of my astronomy professors, for always believing in me and for always being there when I needed help or guidance. And finally, I thank Aldo for giving me the opportunity to work with him without knowing me.

"Esta tesis fue aceptada por la Comisión del Programa de Estudios de Posgrado en Física de la Universidad de Costa Rica, como requisito parcial para optar al grado y título de Maestría Académica en Astrofísica."

Dra. Lela Taliashvilli
Representante del Decano
Sistema de Estudios de Posgrado

Dr. Francisco Frutos Alfaro
Director de Tesis

Dr. Aldo Batta Márquez
Asesor

Dra. Heidy Gutiérrez Garro
Asesora

Dr. Jorge Gutiérrez
Director
Programa de Posgrado en Física

Edwin Santiago Leandro
Candidato

Contents

Resumen

Las observaciones de más de 90 ondas gravitacionales observadas por la colaboración LIGO/VIRGO/KAGRA, han permitido obtener información sobre sistemas binarios compactos, como sus masas y espines. El parámetro de espín efectivo del sistema da información importante para discernir el canal de formación de la binaria. En general, se espera que sistemas binarios que se forman por interacciones dinámicas en sistemas estelares densos, tengan espines efectivos con valores aleatorios entre -1 y 1. Por otro lado, binarias formadas por sistemas aislados deberían tener espines efectivos positivos, a no ser que una "patada natal" en la formación del objeto compacto altere la orientación del mismo, y cambie el valor del espín efectivo como resultado. El objetivo de este trabajo es estudiar la viabilidad de obtener patadas natales grandes en la formación de agujeros negros masivos estudiando explosiones de supernova asimétricas, partiendo de modelos estelares de pre-supernova para estrellas de $21M_{\odot}$ y $28M_{\odot}$, y continuando su movimiento con Simulaciones Hidrodinámicas de Partículas en 3D (SPH). Los resultados muestran que incluso las patadas natales en el orden de $\sim$ 1000 km/s, que son de las más altas encontradas con observaciones, no siempre son capaces de consistentemente darle la vuelta a la orientación de la órbita. Para esto, se requiere que la patada esté direccionada correctamente, y que la energía de la explosión sea bastante alta.

Abstract

The observation of over 90 Gravitational Wave (GW) events by the LIGO-Virgo-KAGRA collaboration, has yielded information of the merger of compact object binaries, such as their individual masses and spins. However, the effective spin parameter obtained from the GW signal provides important information that could be used to discern the binary's formation channel. Overall, binaries formed from dynamic interactions in dense stellar environments are expected to have a random distribution of effective spins between -1 and 1. Meanwhile, binaries formed from the evolution of isolated stellar binaries are expected to have positive effective spins unless there is a large enough natal kick during the compact object formation that could significantly alter the orientation of the individual spins with respect to the binary's angular momentum. We study the viability of obtaining large natal kicks during the formation of massive Black Holes by studying the asymmetric mild explosion of $21M_{\odot}$ and $28M_{\odot}$ pre-supernova stellar models, by means of 3D Smooth Particle Hydrodynamics simulations. Our results show that, even kicks in the order of ~ 1000 km/s, which are among the highest values observed for natal kicks, can't consistently change the orientation of the orbit. These systems would require the kick to be directed correctly, and it would also require for the supernova explosion energy to be quite high.

List of Figures

List of abbreviations

BBH	Binary Black Hole
BH	Black Hole
CE	Common Envelope
GW	Gravitational Waves
LVK	LIGO-Virgo-KAGRA
NK	Natal Kick
NS	Neutron Star
PN	Post-Newtonian
SNE	Supernovae Explosion
SNEfrac	Fraction of the SNE with respect to the binding energy
SPH	Smooth Particle Hydrodynamics

List of symbols

χ_{eff}	Effective Spin Parameter.
v_{sym}	Speed expected after a Natal Kick is reduced from spherically symmetric accretion of mass and momentum.
$\mathcal{M}$	Chirp Mass.
M_1	Mass of the initially more massive star in the Binary System.
M_2	Mass of the initially less massive star in the Binary System.
W	SPH density Kernel.
h_i	Parameters in the Kernel determining its rate of fall.
γ	Adiabatic constant.
N	Number of SPH particles used in a given simulation.

UNIVERSIDAD DE COSTA RICA

SEP Sistema de Estudios de Posgrado

Autorización para digitalización y comunicación pública de Trabajos Finales de Graduación del Sistema de Estudios de Posgrado en el Repositorio Institucional de la Universidad de Costa Rica.

Yo, Edwin Santiago Leandro, con cédula de identidad 305130324, en mi condición de autor del TFG titulado Black Hole Binaries with Natal Kicks

Autorizo a la Universidad de Costa Rica para digitalizar y hacer divulgación pública de forma gratuita de dicho TFG a través del Repositorio Institucional u otro medio electrónico, para ser puesto a disposición del público según lo que establezca el Sistema de Estudios de Posgrado. **SI** [X] **NO** *[ ]

***En caso de la negativa favor indicar el tiempo de restricción: _____ año (s).**

Este Trabajo Final de Graduación será publicado en formato PDF, o en el formato que en el momento se establezca, de tal forma que el acceso al mismo sea libre, con el fin de permitir la consulta e impresión, pero no su modificación.

Manifiesto que mi Trabajo Final de Graduación fue debidamente subido al sistema digital Kerwá y su contenido corresponde al documento original que sirvió para la obtención de mi título, y que su información no infringe ni violenta ningún derecho a terceros. El TFG además cuenta con el visto bueno de mi Director (a) de Tesis o Tutor (a) y cumplió con lo establecido en la revisión del Formato por parte del Sistema de Estudios de Posgrado.

INFORMACIÓN DEL ESTUDIANTE:

Nombre Completo: Edwin Santiago Leandro.

Número de Carné: B66717 Número de cédula: 305130324.

Correo Electrónico: edwin.santiago@ucr.ac.cr.

Fecha: 03/04/2024. Número de teléfono: 87138675.

Nombre del Director (a) de Tesis o Tutor (a): Francisco Frutos Alfaro.

FIRMA ESTUDIANTE

Nota: El presente documento constituye una declaración jurada, cuyos alcances aseguran a la Universidad, que su contenido sea tomado como cierto. Su importancia radica en que permite abreviar procedimientos administrativos, y al mismo tiempo genera una responsabilidad legal para que quien declare contrario a la verdad de lo que manifiesta, puede como consecuencia, enfrentar un proceso penal por delito de perjurio, tipificado en el artículo 318 de nuestro Código Penal. Lo anterior implica que el estudiante se vea forzado a realizar su mayor esfuerzo para que no sólo incluya información veraz en la Licencia de Publicación, sino que también realice diligentemente la gestión de subir el documento correcto en la plataforma digital Kerwá.

Chapter 1

Introduction

1.1 Introduction

Since the first discovery of Gravitational Waves (GWs) in 2015, a new source of information was opened for the study of compact binary systems. The more than 90 GW detected by the LIGO-Virgo-KAGRA (LVK) collaboration also allows us to study the properties and formation channels of Binary Black Holes (BBHs) [1]. From the GW detections, we are able to discern the individual masses of the Black Holes (BHs), as well as their effective spin parameter ($\chi_{\rm eff}$), which can range from -1 to 1 [20, 31] (See Section 1.2.1). Depending on the formation channel of the BBH, different possible distributions of $\chi_{\rm eff}$ are expected [31].

For BBHs that are created from dynamical interactions in dense stellar environments, we expect a random distribution of $\chi_{\rm eff}$ between -1 and 1. This is due to the numerous interactions the BBHs would be experiencing in this environment. [8, 10, 23]. In general, these systems need a mechanism for the BHs to be close enough between them, so that they would merge in a timescale shorter than the age of the Universe. In the case of the BBHs from dense stellar environments, we expect single-binary, binary-binary, and even single-single interactions to help the binary system loose orbital energy, and develop a compact binary as a result. There is no reason to think that these types of interactions would produce BBHs with spins aligned with the angular orbital momentum of the system [10].

Another mechanism for the formation of BBHs would be isolated stellar binary systems. These systems would begin as a stellar binary systems of two OB type stars, which interact with one another throughout their evolution, whenever one of them fills their respective Roche Lobe. The mechanism at play responsible of decreasing the orbital separation of the system is a Common Envelope (CE) that forms when the

second star fills its Roche Lobe, which would reduce the orbital separation to the order of $\sim 10R_{\odot}$. [5, 6]. From these systems, one would expect the individual spins of the binary components to be aligned with the orbital angular momentum. This would mean that, from isolated stellar binary systems, one would initially expect a positive distribution of values for $\chi_{\rm eff}$, unless there is another mechanism at play [23, 31].

For example, it has been proposed that a BH natal kick (NK) of linear momentum can be theoretically able to change the direction of the orbit, and as a result, the sign of $\chi_{\rm eff}$. This NK can be the result of an asymmetry in the Supernova Explosion (SNE) [9, 18]. If the integrated momentum of the SNE tends towards a particular direction, the compact object would go to the opposite direction to conserve linear momentum. These NKs have been observed numerous times in Neutron Stars (NS), but NK detections in BHs are still limited. [30]

Theoretical calculations have been made to calculate how big the NK should be to change the sign of $\chi_{\rm eff}$. [9, 18]. In the simplest scenario one would expect that the NK received by the NS that eventually collapses into a BH would be reduced by the accretion process. However, Janka 2013 proposes that the BH NK would be bigger, by means of a gravitational tug boat mechanism [18].

Janka proposed that the BH NKs should be bigger than the reduced NKs of NSsr after a spherically symmetric accretion of mass and momentum ($v_{\rm sym}$ from now on):

$$v_{\rm BH,f} > v_{\rm sym} \equiv \frac{M_{\rm NS}}{M_{\rm BH,f}} v_{\rm NS}, \tag{1.1}$$

where $v_{\rm BH,f}$ is the final BH speed, $M_{\rm BH,f}$ is the final BH mass and $M_{\rm NS}$ and $v_{\rm NS}$ are the initial NS mass and speed respectively.

Even though the analytic calculations on BH NKs using (1.1) are promising, they do not follow the entire evolution of the accretion of mass and momentum from the asymmetric SN ejecta. In order to study this scenario we will study the process of accretion of material by a newly formed BH located in the center of an exploding star, whose NK will be determined by the asymmetry of the explosion. This will be done by means of 3D Smooth Particle Hydrodynamics (SPH) simulations of pre-supernova stellar models with $21M_{\odot}$ and $28M_{\odot}$. The simulations were run in GADGET with a pre-supernovae stellar model with an asymmetrical distribution of energy as our initial conditions. This would allow us to follow the process of accretion, and the entire evolution of the BH's properties (including the NK). Our objective from this work is to answer if the resulting BH NK after accretion would suffice to change the sign of $\chi_{\rm eff}$.

1.2 Observations from LIGO-Virgo-KAGRA

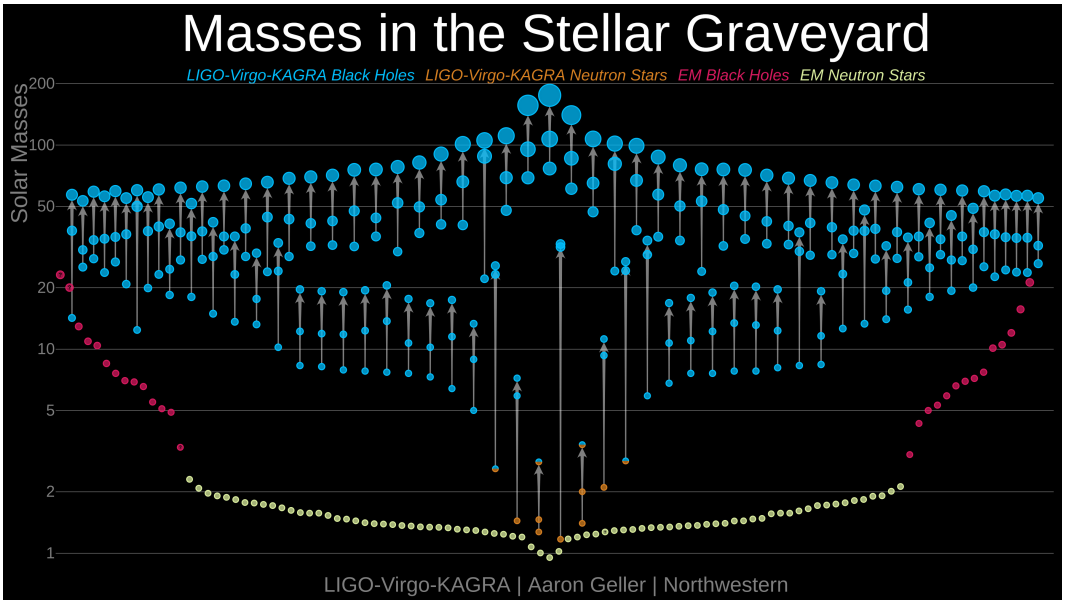

Figure 1.1: List of mergers measured by the LIGO-Virgo-KAGRA Collaboration. The image contains all events discovered until the third observing run (O3). The credits are in the image.

Throughout the years, the LVK collaboration has managed to make over 90 detections of GWs. From these detections, it is possible to obtain their individual masses and spins. However, there are some quantities that are better constrained by the GWs.

The way the properties of the system are obtained, is by computing the inspiral phase and merger with Post-Newtonian (PN) Approximations, and with Numerical Relativity. Not all properties of the system have a direct effect on the waveform of the GW in first order, which makes these properties more difficult to resolve.

1.2.1 Chirp Mass

At the leading order, the evolution of the GW is defined by the Chirp mass:

$$\mathcal{M} \equiv \frac{(m_1 m_2)^{3/5}}{(m_1 + m_2)^{1/5}} \simeq \frac{c^5}{G^3}\left[\frac{5}{96}\pi^{-8/3} f^{-11/3}\dot{f}\right]^{3/5}, \tag{1.2}$$

where m_1 and m_2 constitute the individual masses of the BHs, f is the frequency of the GW, and $\dot{f}$ is its time derivative [1,2]. With following orders in the PN calculation, the mass ratio $q = m_2/m_1 \leqslant 1$ will be at play. This will allow us to discern the individual

masses of the system, but with a higher uncertainty than the Chirp mass and mass ratio. Systems with lower q are better resolved, due to the nature of the GW.

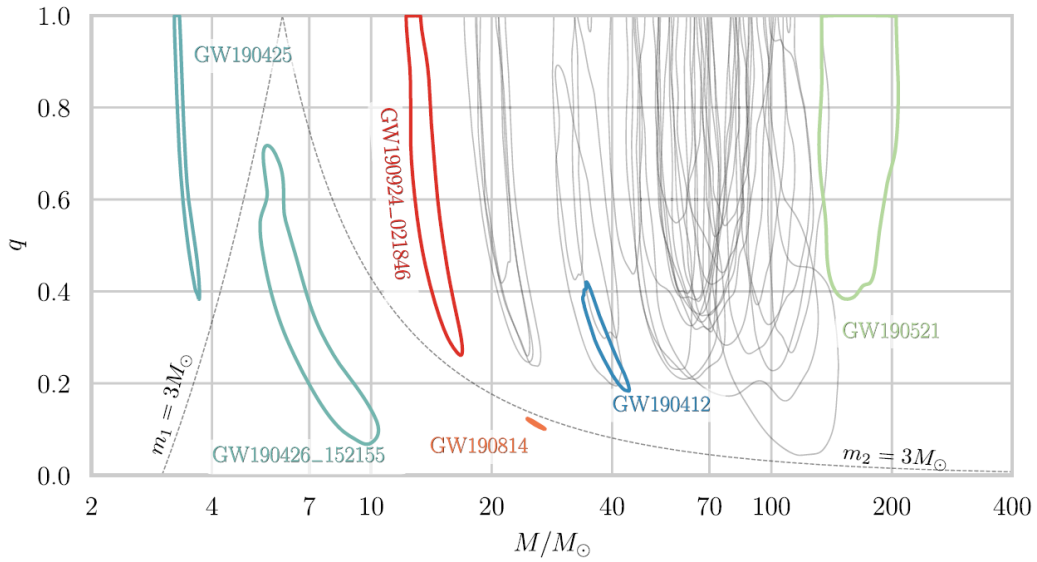

Figure 1.2: Regions of highest probability for the mass ratio parameter on the vertical axis, and the total mass of the system in solar masses on the horizontal axis. The regions represent the areas with 90% of credibility. Image obtained from Abbott et al. 2021 [1].

Figures 1.1 and 1.2 give us an understanding of the types of systems that are normally detected by LVK. Although Fig. 1.1 gives a very clear idea of the mass ranges and how common certain masses are to be detected, it is important to also look at figures like Fig. 1.2 to remember our degree of confidence in some observations. The systems we are interested in Fig. 1.2 are the ones to the right of the $m_2 = 3\mathrm{M}_\odot$ dashed line, from which we can say confidently that correspond to BBHs.

It is important to mention that the majority of systems are reported with higher masses than those measured with electromagnetic observations. There are multiple systems with a probability of having a total mass $> 100\mathrm{M}_\odot$. In particular, the binary system associated with GW190521 has an expected total mass of $163.9^{+39.2}_{-23.5}\mathrm{M}_\odot$ [1].

Most sources seem to have mass ratio confidence regions consistent with mergers of similar mass. With this in mind, it is important to note that the binary associated with GW190412, has an expected mass ratio of $0.28^{0.12}_{-0.06}$, and it is likely for other systems of the ones in Fig. 1.2 to have similar mass ratios, due to the unconstrained nature of the measurements [1].

1.2.2 Effective spin parameter

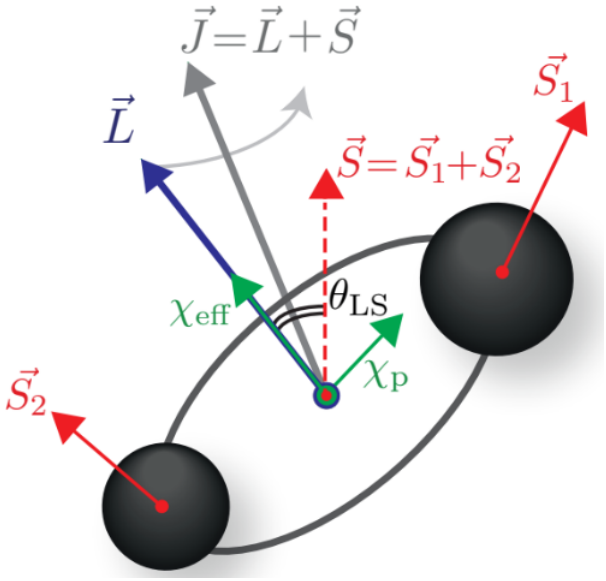

Figure 1.3: Diagram representing what the effective spin parameter represents. Image obtained from Rodriguez et al. 2016 [31].

In the same fashion as the Chirp mass, $\chi_{\rm eff}$ is better constrained than the individual spins of the compact objects. $\chi_{\rm eff}$ also appears in a higher order of the PN approximation, and it also affects the inspiral rate of the binary. The alignment of the spins with the orbital angular momentum increase the number of orbits from an initial separation to merger with respect to the non spinning case. An antialignment, in turn, would decrease the number of orbits [2]. Fig 1.3 represents the BBH system with their individual spins, and the orbital angular momentum. $\chi_{\rm eff}$ is defined as

$$\chi_{\rm eff} = \left(\frac{m_1 \vec{\boldsymbol{\chi}}_1 + m_2 \vec{\boldsymbol{\chi}}_2}{m_1 + m_2} \right) \cdot \hat{\boldsymbol{L}}, \tag{1.3}$$

where $\vec{\boldsymbol{\chi}}_i = c\vec{\boldsymbol{S}}_i/(Gm_i^2)$ is the dimensionless spin parameter, and $\hat{\boldsymbol{L}}$ is a unitary vector in the direction of the orbital angular momentum [31]. Because Gm_i^2/c is the highest possible spin for a BH, χ_i can only take values between 0 and 1. $\chi_{\rm eff}$ can be interpreted as the dimensionless projection of the weighted spins of the BHs, on the orbital angular momentum. This means that the only way to obtain a negative value of $\chi_{\rm eff}$ is by having a misalignment between the total weighted spin and the orbital angular momentum. Therefore, in order to change a positive $\chi_{\rm eff}$ to a negative one by means of a NK, the latter must change the orbital angular momentum vector, so that it points in the opposite direction as before the SNE.

Figure 1.4 shows the regions of 90% certainty for the individual GW detections made between April 1^{st} and October 1^{st} of 2019 [1]. Most of the detections are consistent with values for χ_{eff} close to zero. Eleven of the sources shown in Fig. 1.2 where found to have positive χ_{eff} within the 90% region of credibility. No detection was found with the entire region in the negatives. The lowest region would constitute to the detection GW190514_065416, with expected value $\chi_{\text{eff}} = -0.19^{+0.29}_{-0.32}$ [1].

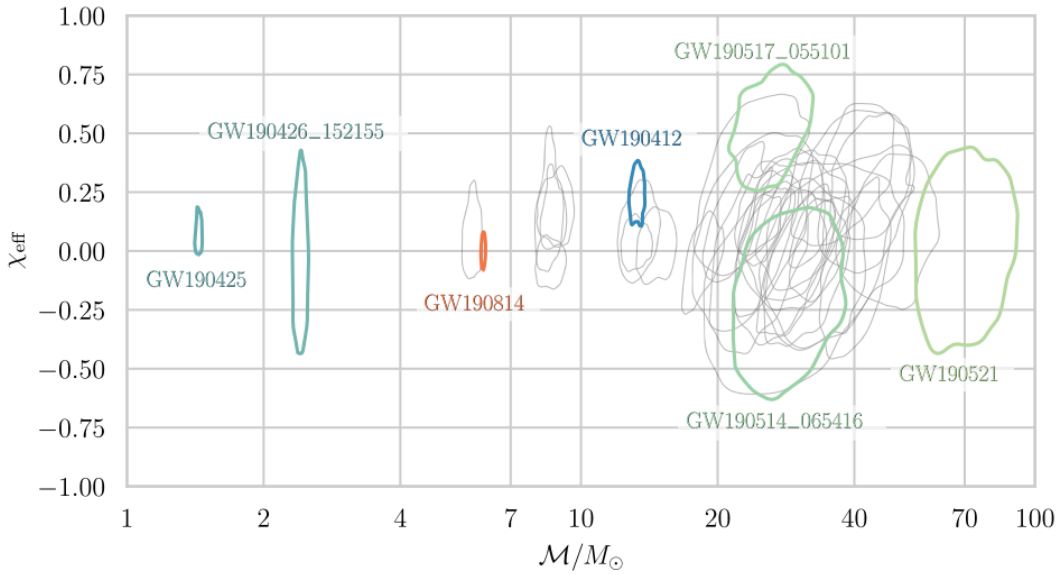

Figure 1.4: Regions of highest probability for the effective spin parameter on the vertical axis, and the chirp mass in solar masses on the horizontal axis. The regions represent the area with 90% of credibility. Image obtained from Abbott et al. 2021 [1].

That said, the sizes of the regions tells us that most of the observations can either be positive or negative, and remain in the certainty range. It is important to find out if it is possible for isolated stellar binary systems with a NK to end up in the negative region, because this can give us further information on the formation channel of some detections in the future.

1.2.3 Precession spin parameter

It is also possible to measure the projection of the BH spins on the orbital plane. These components would lead to a precession of the spins, and the parameter is called the precession spin parameter χ_{p}. Because of this precession, χ_{p} introduces modulations in the strain amplitude and phase of the GW [1, 2]. There is some evidence of precession in some systems, but this quantity is less present in our current observations.

The equations of motion for the precession of the orbit is

$$\dot{\vec{\boldsymbol{L}}} = \frac{G}{c^2 r^3}(B_1 \vec{\boldsymbol{S}}_{1\parallel} + B_2 \vec{\boldsymbol{S}}_{2\parallel}) \times \vec{\boldsymbol{L}}, \tag{1.4}$$

$$\dot{\vec{\boldsymbol{S}}}_i = \frac{G}{c^2 r^3} B_i \vec{\boldsymbol{S}}_{i\parallel} \times \vec{\boldsymbol{L}}, \tag{1.5}$$

Where $\vec{\boldsymbol{S}}_{i\parallel}$ is the projection of the spin in the orbital plane, $B_1 = 2 + 3q/2$, and $B_2 = 2 + 3/(2q)$. From these definitions, one can define the precession spin parameter as

$$\chi_{\rm p} = \frac{c}{B_1 G m_1^2} \max\left(B_1 \boldsymbol{S}_{1\parallel}, B_2 \boldsymbol{S}_{2\parallel}\right) > 0, \tag{1.6}$$

where an $\chi_{\rm p}$ of 0 corresponds to zero precession, and an $\chi_{\rm p}$ of 1 corresponds to maximum precession. Part of the reason that this is a more difficult quantity to obtain is because it appears in higher order terms in the PN approximation, and because it is better constrained when the masses are significantly different. Researchers have constrained $\chi_{\rm p}$ for detections with different enough masses, for instance, with GW190814, which has a $q = 0.112^{+0.008}_{-0.009}$. However, this is not a common parameter to obtain, specially with systems of similar masses.

1.3 Overview of the thesis

In Chapter 2, we will be discussing the BBHs formation mechanisms and characteristics. This will include both the isolated case, the dense stellar environments and the conditions for a BBH to be detectable. Next, we will be discussing NKs, including the instantaneous mass loss approximation, the observed distribution of NKs and the gravitational tug boat mechanism proposed in Janka 2013. [18] In Chapter 3, we will be discussing the theory behind SPH simulations and GADGET, as well as the construction of the initial conditions we set up for our simulations, along with some convergence tests. In Chapter 4, we will analyze our results, by dividing them in the properties of an isolated BH after accretion, and the properties of the binary systems. In Chapter 5, we present a summary and our conclusions.

1.4 Objectives

1.4.1 General Objective

Study the viability of obtaining large natal kicks during the formation of massive black holes in asymmetric mild supernova explosions.

1.4.2 Specific Objectives

- Carry out hydrodynamical simulations of the accretion of asymmetric supernova explosions with a central black hole.
- Explore the effect of asymmetric supernova explosions with distinct properties in the resulting magnitude of black hole natal kicks.
- Calculate the black hole properties during the process of accretion.
- Compare the physical properties obtained from the simulations with the analytical calculations that assume spherical symmetry and an instantaneous loss of mass.

Chapter 2

Black Hole Binaries Formation Mechanisms and Properties

2.1 Formation and Evolution of Compact Black Hole Binaries

The formation and evolution of compact BBHs can happen either in isolated systems, or in dense stellar environments. For both cases, it is important to understand the isolated case. The formation in dense stellar environments can be differentiated from the isolated case by the interactions that can occur between individual systems (although unlikely), individual and binary systems and between two binary systems. Although numerous mechanisms were proposed for the isolated systems, the LVK observations indicate the evolution through a CE to be the most likely formation mechanism for the BBHs observed through GWs [5]. We will present a short description of the important details, but if the reader wants to learn more, there are multiple references describing the formation and evolution of compact systems in more depth [8, 13, 23, 26].

2.1.1 Isolated stellar binaries

Compact BBHs are expected to form from a binary system of two massive (OB) stars. The standard path for this binary system is summarized in Fig 2.1. The initial system of two OB stars would circularize their orbit due to tidal interactions. With the passage of time, the more massive star (which we will call M_1 for future reference) is expected to consume its Hydrogen faster than the less massive star (which we will call M_2), and expand as a result. This would, in turn, overfill the Roche Lobe and initiate the first transfer of mass for the binary system. Some of the mass would be lost, while the rest

of it would be absorbed by M_2. It is also possible, depending on the individual masses, for the transfer of mass in this stage to happen with a CE phase. M_1 will continue transferring its outer Hydrogen envelope to M_2, until it is lost [26].

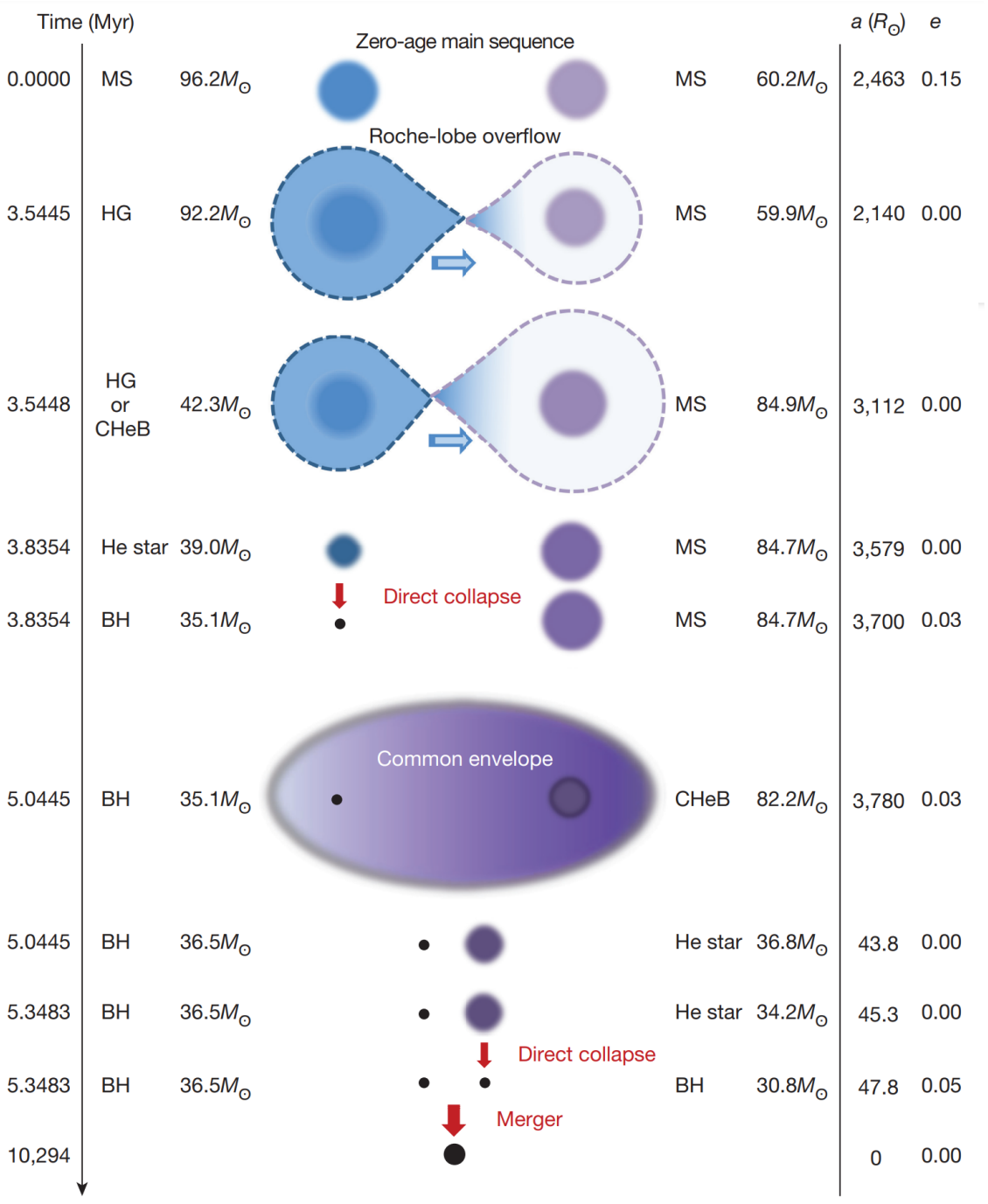

Figure 2.1: Description of the evolutionary path that an isolated binary system may take. a represents the separation at a given stage and e the eccentricity. Image obtained from Belczynski et al. 2016 [6].

After the initial transfer of mass is finished, M_1 would end up as a naked Helium core. Depending on the mass of M_1 after accretion, it could be observed as a Wolf Rayet star. In turn, M_2 would end up as the more massive star in the following stages of the evolution of the binary system. M_2 is also expected to gain a significant amount of angular momentum due to the mass transfer, converting it into a rapidly rotating Be star. M_1 will eventually explode as either a Core-Collapse SNE or an Electron Capture Super Nova. M_1 will become either a NS or a BH (compact object, from now on) [23, 26].

It is possible for the system not to survive the SNE. If it does, the system would be a rapidly rotating Be star with a compact object. The orbital eccentricity after the SNE is expected to be high, which means that some accretion will occur when M_2 goes through the periastron. This process will continue as M_2 evolves, expands and fills its Roche Lobe. Due to the large mass ratio between the systems, a CE will inevitably form [8, 23, 26].

This CE is very important for the evolution of the binary, since it is the primary mechanism allowing for the system to decrease its orbital separation and orbital period significantly (which is denoted as hardening). The basics of the CE would be as follows: When a CE forms, this will form a drag force acting on the compact object orbiting inside the envelope, forcing it to spiral in towards the core of the massive star. In the meantime, this drag force will inject energy into the envelope (which comes from the binary's lost orbital energy). As a final result, either the envelope gains sufficient energy to be ejected and yields a significantly hardened binary composed of the compact object and the stellar core (an He-star), or the compact object continues spiraling in until it merges with the stellar core in a rapidly rotating single object. There are still open questions about the details regarding how the CE forms and evolves. We will leave the reader with further material explaining the topic in much more depth [12, 17].

If the outcome of the CE phase is a close binary system (compact object and He-star), eventually the star will collapse into a BH. However, before BH formation, the collapsed core will form a proto NS, going through a stage in which there could be enough energy production to power a mild supernova explosion that ejects some of the stellar material. Nevertheless, since this outer material continues falling onto the NS, it will eventually collapse into a BH. This is the stage we will study by means of SPH simulations, consisting of a low mass BH formed by the collapse of the core, surrounded by a mild SNE that travels through the outer layers of the star.

In this scenario, the disruption of the binary system could occur. The binary system will be disrupted if the mass loss due to the explosion exceeds half of the total mass

of the binary. A NK can make things worse, since adding a velocity to the BH in the right direction can further help to unbind the system. Therefore, in order to obtain binaries at the end of this process, it is important to consider NKs with the right direction and magnitude to avoid the disruption of the binary system. At the end of our simulations we will end with a BH binary, whose properties will be determined by the initial properties of the system and the properties of the SNE. Since the formation of both compact objects comes from the collapse of He-stars, which started as OB stars, one would expect the compact objects to be of similar masses [13, 26, 34].

An important aspect to highlight about these systems is that we expect the stars that form massive BBHs to be of low metallicity. The reason behind this phenomenon has to do with the opacity of the star. Very massive stars tend to have very strong stellar winds that reduces the mass of the star throughout its evolution. How strong is this effects depends strongly on the atomic line opacity, which diminishes when the star has a lower metallicity. These means that lower metallicity stars tend to maintain more of their mass before the core collapse. As a result, they are more likely to produce the higher mass BBHs that tend to form under this scenario. [10]

Another property relevant for this work is that, as mentioned before, M_1 is expected to give a significant amount of its angular momentum to M_2 during the mass transfer process. This is expected because the mass transfer begins once M_1 turns into a giant star, and we expect most of the angular momentum in that moment to be in the outer layers, the ones that are transferred to M_2. Therefore, the first born BH should have a spin consistent with 0. The spin of the second-born BH is dependent on the stellar winds and tidal interactions of M_2. Although there were previous studies suggesting that the spin of the second-born BH is either consistent with 0 or maximally spinning, more detailed studies show that the second-born BH can have any spin from 0 to 1, depending on the properties of the system. At low metallicities, the range of orbital periods that allows values significantly different than the extremes (0 or 1) is large enough to be taken into account [5, 10, 29].

2.1.2 Formation in dense stellar environments

In dense stellar systems, encounters and interactions with other unitary or binary systems become important to describe the populations of compact binary systems expected from these environments. The mechanisms discussed previously continue to apply, but the system no longer evolves in isolation. Reduction or increase of the orbital period and separation (softening or hardening of the system, respectively), formation of new binary systems, or even encounter-induced binary mergers can happen due to the fact

that close encounters are much more common. We are defining dense stellar environments as $\gtrsim 10^3$ stars/pc^3 [8, 23].

In the case of single-single interactions, it is possible to form a new binary system if the pericenter of the encounter is small enough, so that the tidal interactions dissipate sufficient kinetic energy to bound the system. The fraction of the energy that should be dissipated with tidal interactions to bound successfully the system is in the order of $\sim (v_{\rm a}/v_{\rm p})^2$, where $v_{\rm a}$ is the relative speed at apocenter, and $v_{\rm p}$ at pericenter. From this, one can conclude that this mechanism favors the creation of binary systems with big ratios between pericenter and apocenter velocities, and thus highly eccentric systems. Having said that, it is thought that this is not the most likely mechanism for the creation of binary systems in dense stellar environments because the stars must get really close between them [8].

In three body encounters, it is possible for the least massive star to gain kinetic energy from the others and, as a result, bound the more massive stars of the event. Three body interactions dominate more at densities closer to the cores of Globular Clusters. Although Ivanova et al. 2010 showed that binary formation could be relevant in the formation process of certain types of compact binaries, in general, interactions between already formed binary systems and other stars or binaries are the main mechanism in which large numbers of relativistic binaries in globular clusters are expected to form [8, 16].

In the case of binary-single interactions, it is possible to either harden or soften the system depending on the kinetic energy of the single star, relative to the system. Stars with lower kinetic energy than the magnitude of the binding energy of the system (which we will call $\rm E_b$ for future reference) are expected to harden the system, while the contrary would happen for stars with higher kinetic energy relative to the binary system. A star with higher kinetic energy than $\rm E_b$ would most likely donate kinetic energy to the binary, and this ends up softening the system. This means that the lower the period of a binary system is, the higher would be $\rm E_b$, and the likelihood of encountering a star with kinetic energy lower than $\rm E_b$ would increase further and further. The opposite would occur for binary systems with higher and higher orbital period. Therefore, we have a consistent mechanism for creating by this manner compact binary systems in dense stellar environments. Even more cases can be analyzed with interactions between more and more stars, but the probability of these events occurring would be smaller and smaller as a result [8, 23].

The literature agrees that one should expect an isotropic distribution of $\chi_{\rm eff}$, due to all the space of viable interactions, in such a dense environment. Rodriguez et al. 2018

showed in PN simulations that the distribution is indeed isotropic, and that globular clusters are capable of forming BBH with $\chi_{\rm eff} < 0$, regardless of the initial spins of the individual BHs. It is also possible to a second generation of BBHs with large spins $\chi_{\rm eff} \sim 0.7$ from a first generation of low spin BHs.

2.1.3 Time of merger and detectable Black Hole Binaries

Now that we understand the formation process of BBH, it is important to see if they are detectable. A first important aspect to consider, is that it takes time for the BBH to irradiate its orbital energy through GWs, so they need to be close enough so that they will merge before the Hubble time.

A binary system with BH masses M_1 and M_2 and a circular orbit will irradiate energy at a rate given by

$$\frac{dE}{dt} = -\frac{32}{5}\frac{G^4}{c^5}\frac{M_1 M_2 (M_1 + M_2)}{a^5}, \tag{2.1}$$

where a is the orbital separation. From this equation, it is straightforward to prove that the time of merger is given by

$$t_{merger} = \frac{5}{256}\frac{c^5}{G^3}\frac{a_0^4}{M_1 M_2 (M_1 + M_2)}, \tag{2.2}$$

where a_0 is the initial separation of the system. If the BBH has an initial eccentricity e_0, then the time of merger must be multiplied by the factor $f(e_0)$, where

$$f(e) = \frac{48}{19}\frac{(1-e^2)^4}{e^{48/19}\left(1+\frac{121}{304}e^2\right)^{3480/2299}}\int_0^e \frac{\left(1+\frac{121}{304}e'^2\right)^{1181/2299}}{(1-e'^2)^{3/2}} e'^{29/19} de' \tag{2.3}$$

This limits how separated the system can be, for their merger to be detectable [26]. Fig. 2.2 shows the range of possible maximum orbital separations a BBH can have to be detected in the Hubble time. The figure assumes a circular binary system. It could be the case that the NK from the second SNE can alter the eccentricity of the system. However, as the orbital separation decreases due to the gravitational radiation, the orbit is expected to become more and more circular. For this reason, the expectation is that when the LVK collaboration detects a GW source, the BBH orbit should be close to circular [1, 10].

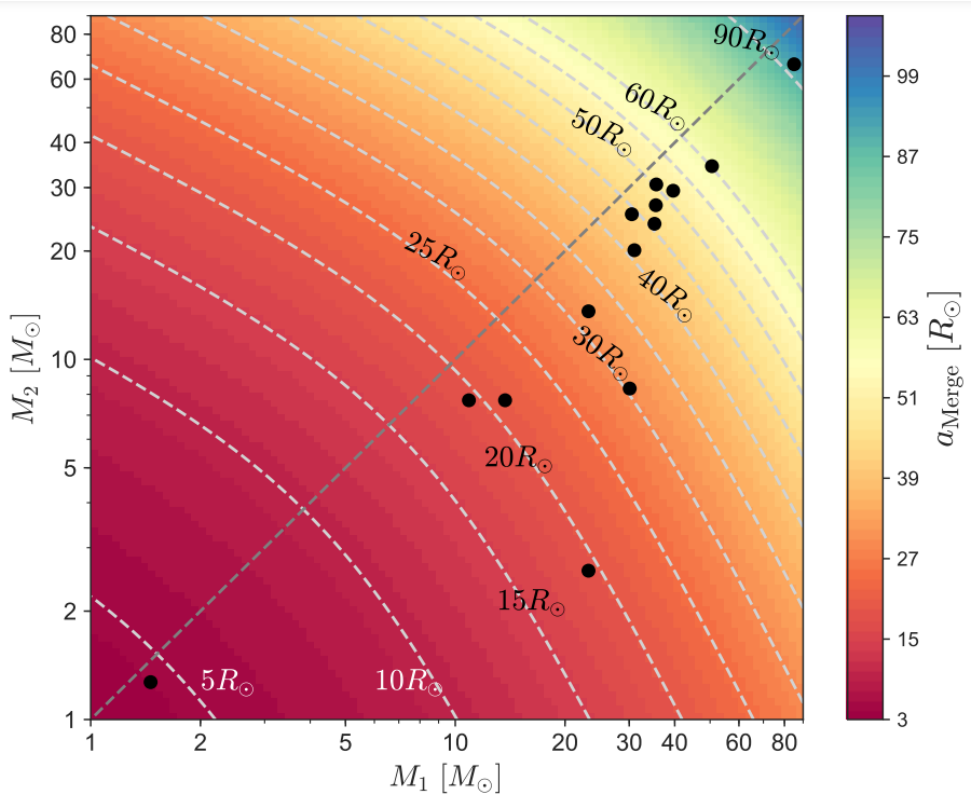

Figure 2.2: Maximum separation a circular binary system can have, so that they merge in the Hubble time, for different masses.

Another important aspect to take into account is the sensitivity of our current instruments, and the type of BBHs that they are most likely to detect. The current observatories have more sensitivity to systems in the local universe ($z_{\rm observed} \sim 0$), and systems with higher chirp masses. Because of the relationship between lower metallicities and higher masses that we mentioned before, the observatories are more likely to encounter systems with lower metallicity. ($z_{\rm formation} \gtrsim 2-3$), which means a long merging timescale. Qin et al. 2018 concludes that because of the anti-correlation that has been found between the time of merger and $\chi_{\rm eff}$, this can be a reason why we are seeing more systems with low $\chi_{\rm eff}$, and that future observations with higher sensitivity may lead to more detections with higher $\chi_{\rm eff}$ [5, 10]. Although it is true that future observations may lead to more detections with higher $\chi_{\rm eff}$, the anti-correlation depends on either tidal locking, or strong tidal interactions, which may not happen in all binaries. It is important to mention here that our work focuses on the easiest systems to turn around their orbit, so we are working with a separation close to the limits shown in Fig. 2.2.

2.2 Natal Kicks

In this section, we will be discussing the proposed mechanisms behind NKs, the analytical calculations, and the observations that we have so far. To begin, the idea behind a NK is that there is an asymmetrical emission of energy in the rest frame of the star. A result of this asymmetry would be a final velocity of the compact object in this frame, to conserve linear momentum. There have been multiple mechanisms proposed for the formation of this asymmetry, the most prevalent ones being an asymmetrical emission of neutrinos, and an asymmetric mass ejection due to hydrodynamical processes. [18]

2.2.1 Instantaneous Mass Loss Approximation

Because the SNE occurs in a dynamical timescale, which is much smaller than the orbital period of the system, normally it is assumed in the literature that the SNE, the NK, and the changes in the system the NK produces, are instantaneous. Here, we present the main relations of the binary system after the NK. This section closely follows the work of Brandt & Podsialowski 1995 [9].

We can begin by considering an orbital system with masses M_1 and M_2. After the SNE, M_1 would instantaneously produce a remnant of mass M_1'. We begin with a circular orbit with initial orbital separation a_0. Let θ be the angle of inclination from the orbital plane of the kick velocity, and let ϕ be the angle in the orbital plane from the orbital velocity of M_1 to the kick velocity. If we define the quantities

$$\tilde{m} = \frac{M_1 + M_2}{M_1' + M_2}, \tag{2.4}$$

and

$$\tilde{v} = \frac{v_{\text{kick}}}{v_{\text{orb}}}, \tag{2.5}$$

then the new orbital energy of the system after the SNE, in the frame of the new center of mass, would be

$$E' = -\frac{GM_1'M_2}{a}\left[2 - \tilde{m}\left(1 + 2\tilde{v}\cos\phi\cos\theta + \tilde{v}^2\right)\right]. \tag{2.6}$$

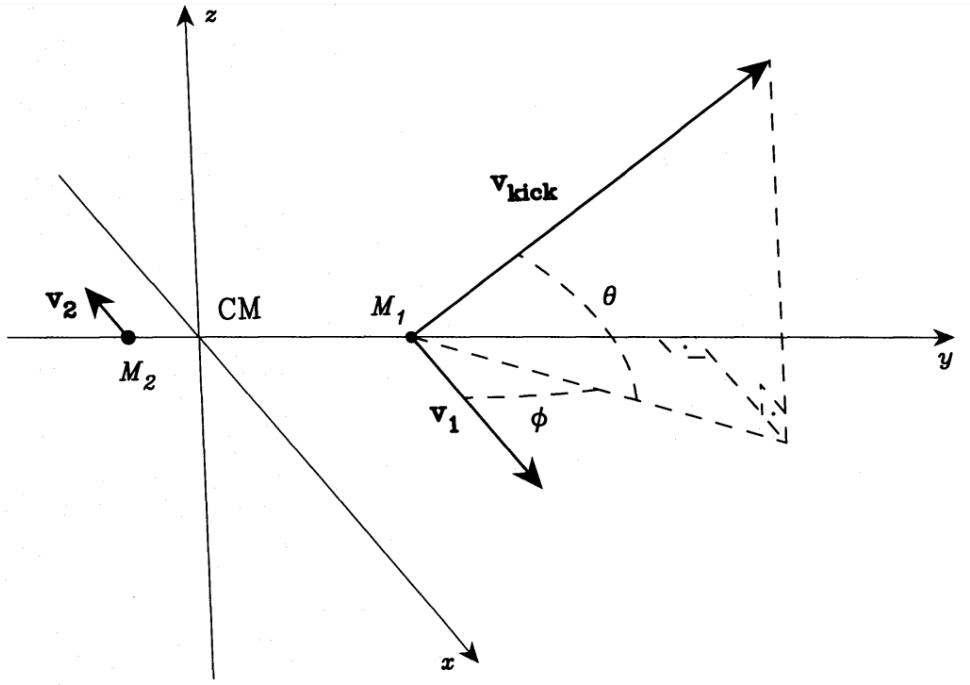

Figure 2.3: Diagram of the orbital system, and the direction of the kick velocity. Image obtained from Brandt & Podsialowski 1995 [9].

Now, if we equate it to the standard orbital energy of a binary system, we can easily find the relation

$$\frac{a}{a'} = 2 - \tilde{m}[1 + 2\tilde{v}\cos\phi\cos\theta + \tilde{v}^2], \tag{2.7}$$

which allows us to find the final separation of the binary. The final eccentricity can be obtained using the relation

$$e^2 = 1 - \tilde{m}\left[2 - \tilde{m}\left(1 + 2\tilde{v}\cos\phi\cos\theta + \tilde{v}^2\right)\right]\left[(1 + \tilde{v}\cos\phi\cos\theta)^2 + (\tilde{v}\sin\theta)^2\right]. \tag{2.8}$$

Because we want the system to remain bound after the SNE, we require that

$$\tilde{v} < \sqrt{1 + \frac{2}{\tilde{m}}} \tag{2.9}$$

and

$$\cos\phi\cos\theta < \frac{1}{2\tilde{v}}\left[\frac{2}{\tilde{m}} - 1 - \tilde{v}^2\right]. \tag{2.10}$$

The lowest possible value of $\cos\phi\cos\theta$ is achieved when the kick is in the orbital

plane and going in the direction against the orbital velocity. The L_z of the system after the SNE in Fig. 2.3 is given by

$$L_z = -\frac{M_1' M_2 a}{M_1' + M_2}(v_{\text{orb}} + v_{\text{kick}} \cos\theta \cos\phi), \tag{2.11}$$

where it is also clear that the easiest path towards changing the direction of the orbit, is with the kick's direction being opposite to the orbital velocity [9, 34]. Note that in Fig. 2.3, the original orbit is going clockwise. In our initial conditions, we will define the original orbit as going counterclockwise, so that a change in the direction of the orbit will be seen as a negative L_z.

2.2.2 Natal Kick Observations

There have been multiple observations on the NKs of NSs. Fig. 2.4 shows the distribution of these observations. The literature is consistent in finding a bimodal distribution for the NKs of NSs. The general finding is that most NKs have a speed of $\lesssim 300$ km/s, but there are a significant amount of NKs that follow a distribution that peaks in $\sim 300 - 500$ km/s. Higher speed NKs (in the range of ~ 1000 km/s) are unlikely but possible. Since the highest NKs observed are in this range [15, 38], it would be fair to say that a mechanism that relies in NKs in the order of ~ 1000 km/s cannot be taken as something that happens often.

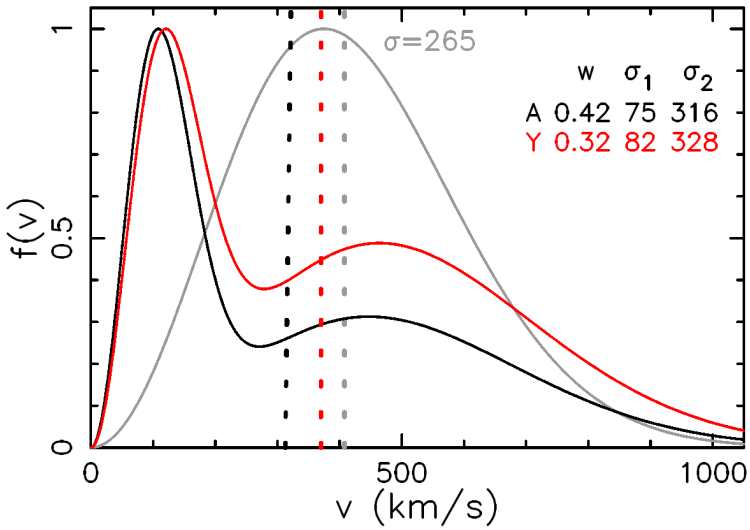

Figure 2.4: Distribution of observed young pulsars. The grey line is the data reduced to a single maxwellian distribution. σ_1 and σ_2 represent the mean of each of the peaks in the bimodal distribution. Figure obtained from Verbunt et al. 2018 [38].

2.2.3 Black Hole Natal Kicks and Gravitational Tug Boat Mechanism

Even though there is enough findings on the NKs of NSs, the BH case is much more difficult to measure, and we still do not have reliable data to talk about the possible distribution of BH NKs. Repetto et al. 2012 considered the distribution of BH low-mass X-ray binaries in the galaxy, and concluded that BH NKs must be taking place in order to move the systems to such large distances outside of the galactic plane [30].

As a first approximation, one would expect a BH NK distribution with smaller velocities than the one for NSs. This is due to the fact that, under the assumption of spherically symmetric accretion, $v_{\rm BH} = v_{sym}$ (see Eq. 1.1). However, Janka 2013 proposes otherwise. From Fig. 2.5, it is easy to see that an asymmetrical emission of material will give a NK to the compact object. However, another interesting mechanism to note is that the denser and slower material will have a gravitational effect on the compact object. This distribution of material will end up accelerating the compact object more towards the direction of the original kick in momentum. This can, in turn, give bigger NKs for the BHs than expected from symmetrical accretion of material. In other words, it would be possible under this mechanism, to have a $v_{\rm BH} > v_{sym}$.

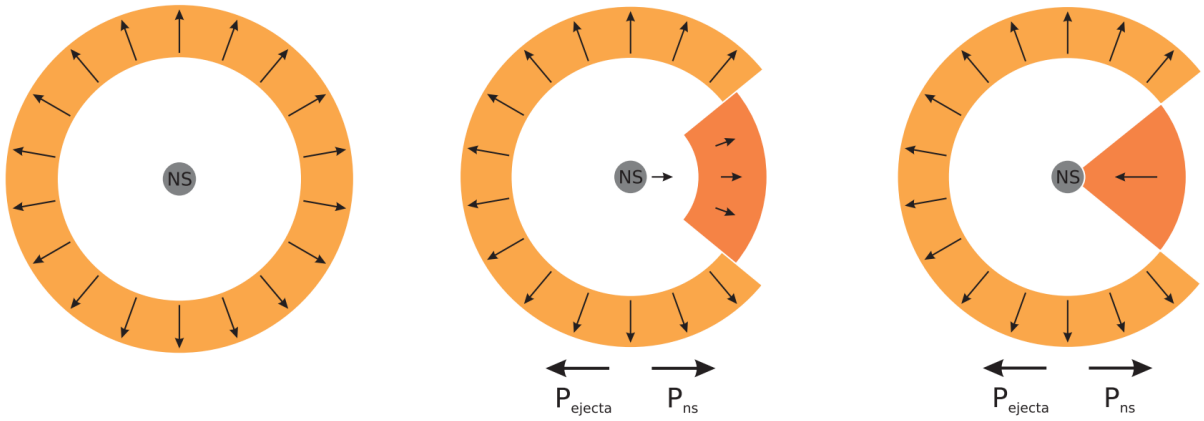

Figure 2.5: Diagram of the NK forming as a result of an asymmetrical ejection of matter. Image obtained from Janka 2013 [18].

Chapter 3

Numerical methods and initial conditions

Our method for studying BBHs with NKs is by running 3D SPH simulations with the help of GADGET (**GA**laxies with **D**ark matter and **G**as int**E**rac**T**). This chapter will explain the basics of both SPH simulations and GADGET, how the initial conditions are constructed, and the convergence tests that were made. However, in a similar fashion to the previous chapter, there will be a lot of details left out of this summary, and we encourage the interested reader to seek out further references describing SPH simulations and GADGET as a whole [27, 28, 36, 37].

3.1 Smooth particle hydrodynamics (SPH)

SPH simulations are best described as a Lagrangian based approach to solving the hydrodynamic equations of motion, by means of modelling the system as a collection of particles. The idea behind it would be that, if the collection of particles is representing a continuous distribution of matter, then the more particles you add to the system, the better this collection would represent the continuous case and the better the simulation would be as a result. Each of the particles would have all of the relevant hydrodynamical properties (position $\vec{\boldsymbol{r}}_i$, velocity $\vec{\boldsymbol{v}}_i$, acceleration $\vec{\boldsymbol{a}}_i$, local density ρ_i, specific entropy s_i, internal energy u_i, local pressure P_i) [3, 27].

The first step would be to compute accurately the density of a system of particles, so that the equations of motion can be defined. There are a number of ways to compute the density of the system of particles, but the way it is normally done in SPH is by defining a Kernel W such that

$$\rho_i(\vec{\boldsymbol{r}}) = \sum_{j=1}^{N_{\mathrm{SPH}}} m_j W(\vec{\boldsymbol{r}}_i - \vec{\boldsymbol{r}}_j, h_i), \tag{3.1}$$

where h_i are parameters in the Kernel that determine the rate of fall, and N_{SPH} is the number of smoothing neighbors. It is important to mention that the Kernel must be normalized over the entire volume,

$$\int_V W(\vec{\boldsymbol{r}}' - \vec{\boldsymbol{r}}_j, h_j) dV' = 1, \tag{3.2}$$

and the parameters can be restricted with the equation

$$\frac{4\pi}{3} h_i^3 \rho_i = N_{\mathrm{SPH}} \overline{m}, \tag{3.3}$$

where $\overline{m}$ represents the average mass. This is not the only way to define the smoothing lengths h_i or the number of smoothing neighbors N_{SPH}. Once the density function is properly defined, one can also define the Lagrangian and, with the rest of the hydrodynamical formalism, compute the equations of motion [27, 36].

3.2 GADGET

GADGET (**GA**laxies with **D**ark matter and **G**as int**E**rac**T**), is defined initially as a simulation code which can be utilized for N-body/SPH simulations regarding both self gravitating systems, and cosmological simulations [37]. GADGET-2, which is the version that will be used in this work, is defined as a TreeSPH code. "Tree" here is referring to the tree algorithm; which is a hierarchical grouping that allows GADGET-2 to calculate the gravitational interactions with fewer computations [36]. In any case, GADGET-2 allows us to run 3D SPH simulations by following the gravitational force between the interacting gas and the BHs, and also the hydrodynamical evolution of the system simultaneously [3].

The Kernel that GADGET-2 utilizes for defining the density function is the following:

$$W(r,h) = \frac{8}{\pi h^3} \begin{cases} 1 - 6\left(\frac{r}{h}\right)^2 + 6\left(\frac{r}{h}\right)^3 & \text{if } 0 \leq \frac{r}{h} \leq \frac{1}{2}, \\ 2\left(1 - \frac{r}{h}\right)^3 & \text{if } \frac{1}{2} < \frac{r}{h} \leq 1, \\ 0 & \text{if } \frac{r}{h} > 1. \end{cases} \tag{3.4}$$

Taking this into account, we can define the interaction potential φ, which comes

from solving the Poisson equation, and we can then define the Hamiltonian as

$$\mathrm{H} = \sum_i \frac{p_i^2}{2m_i a(t)^2} + \frac{1}{2}\sum_{i,j} \frac{m_i m_j \varphi(\vec{\boldsymbol{r}}_i - \vec{\boldsymbol{r}}_j)}{a(t)}, \tag{3.5}$$

with $a(t)$ the scale factor, which for our purposes, will be equal to 1 [36].

If we abbreviate the kernel notation as $W(\vec{r}_i - \vec{r}_j, h_i) = W_{ij}(h_i)$, then we can write the SPH equations of motion as

$$\frac{d\vec{\mathbf{v}}_i}{dt} = -\sum_{j=1}^{N} m_j \left[f_i \frac{P_i}{\rho_i^2} \overrightarrow{\boldsymbol{\nabla}}_i W_{ij}(h_i) + f_j \frac{P_j}{\rho_j^2} \overrightarrow{\boldsymbol{\nabla}}_i W_{ij}(h_j) \right], \tag{3.6}$$

where the coefficients f_i are defined as

$$f_i = \left(1 + \frac{h_i}{3\rho_i} \frac{\partial \rho_i}{\partial h_i} \right)^{-1}. \tag{3.7}$$

and the pressure is given by $P_i = s_i \rho_i^{\gamma}$ [27, 36].

As well as the previous physics mentioned, GADGET-2 uses a viscous force to avoid discontinuities and divergences when particles get too close to each other. This viscous force is defined as

$$\left.\frac{d\vec{\mathbf{v}}_i}{dt}\right|_{\mathrm{visc}} = -\sum_{j=1}^{N} m_j \Pi_{ij} \overrightarrow{\boldsymbol{\nabla}}_i \overline{W}_{ij}, \tag{3.8}$$

where Π_{ij} corresponds to the artificial viscosity. In the case of GADGET-2, this viscosity takes the form

$$\Pi_{ij} = \begin{cases} -\frac{\alpha}{2} \frac{(c_i + c_j - 3w_{ij}) w_{ij}}{\rho_{ij}} & \text{if } \vec{\mathbf{v}}_{ij} \cdot \vec{\mathbf{r}}_{ij} < 0, \\ 0 & \text{otherwise,} \end{cases} \tag{3.9}$$

with α the coefficient that determines the strength of the viscosity, c_i the mean sound in the region, and $w_{ij} = \vec{\mathbf{v}}_{ij} \cdot \vec{\mathbf{r}}_{ij} / |\vec{\mathbf{r}}_{ij}|$ [36].

3.3 Initial conditions

3.3.1 Pre-supernova stellar models

We want to study the viability of obtaining large natal kicks during the formation of massive BHs. To achieve this goal, our objective is to study the asymmetric mild explosion of $21\mathrm{M}_{\odot}$ and $28\mathrm{M}_{\odot}$ pre-supernova stellar models (from [40]), by means of 3D

Smooth Particle Hydrodynamics simulations. This would model the second SNE that happens in Fig 2.1. Woosley & Heger 2006 ran their stellar models with the KEPLER implicit hydrodynamics package. The models assume spherical symmetry. From the range of stars that were simulated, we utilize stars with higher mass and very low metallicity. As mentioned before, our choice for systems with higher mass and low metallicity is due to the types of systems that are expected to be detected from GWs.

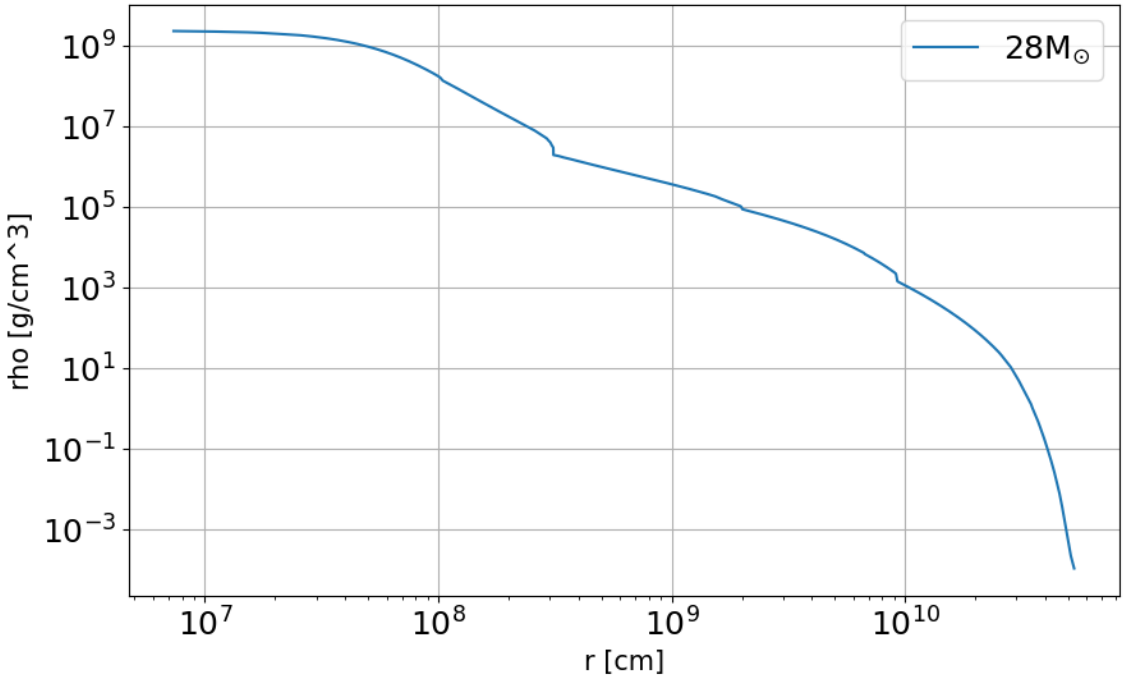

Figure 3.1: Star density distribution of the $28M_{\odot}$ pre-supernova stellar models obtained from Woosley & Heger 2006 [40].

The star is given an orbital period of 0.5 days, assuming it does not have a particularly high rotation. This was done for two reasons. The first one is that the focus of this research is to study whether the NK will turn around the orbital motion of the binary system, and this is independent from the amount of rotation of the individual star. The second reason is that, if we add a very high rotation to the system, then the spherical symmetry assumed by the Woosley & Heger 2006 models would not apply. Future research can take this phenomenon into account.

3.3.2 Natal Kick construction

In order to build our initial conditions, we need more particles in the center of the star, and less particles in the outer layers, in proportion to the local density of the pre-supernova stellar model at a given radius ($\rho(r)$ from now on). The models are mapped

into a 3D (almost) spherically symmetric distribution of SPH particles, in proportion to $\rho(r)$ (See Fig 3.1). This is done by distributing N_{shell} particles on spherical shells according to the discrete surface mapping used in HEALPix [11]. The number of SPH particles N_{shell} at a radius r, is given by $\rho(r)$ and the particle mass [4]. This spherical shells are also rotated randomly to avoid any artificial alignment in the particle distribution.

Once we have the distribution of particles representing the pre-supernova stellar model, then the innermost particles, corresponding to the central $3M_{\odot}$, are replaced by a single sink particle in the center which represents the BH. Then, the explosion energy is added as kinetic energy to the innermost particles around the BH. In total, the kinetic energy is given to $1M_{\odot}$ around the BH. The explosion energy is distributed following a Gaussian distribution whose maximum is located along a certain axis and decreases with the polar angle towards a smaller value (Fig 3.2).

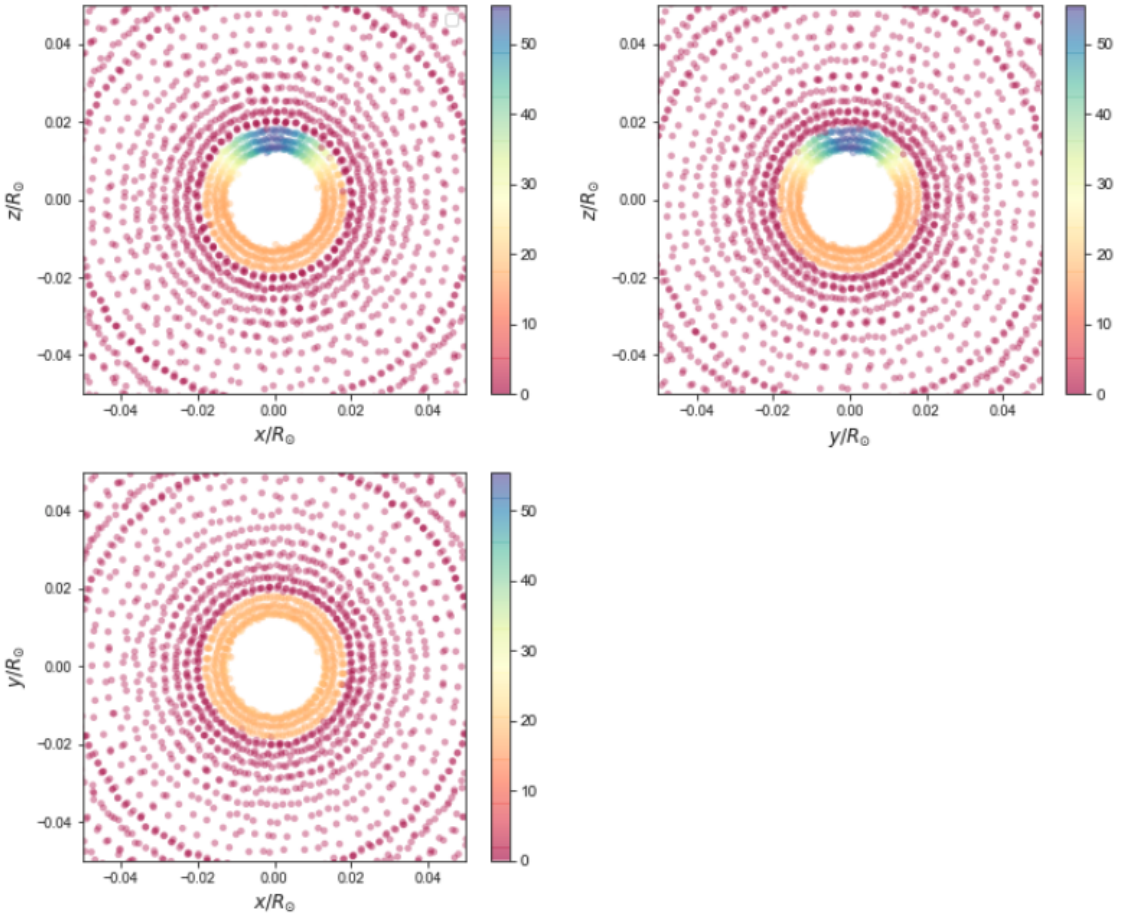

Figure 3.2: Radial velocity of particles surrounding the BH. The asymmetry in the kinetic energy distribution points towards the z axis. The colorbar represents radial speed in thousands of km/s.

In our simulations we choose as free parameters the energy of the explosion, the amplitude of the Gaussian distribution, and the width of the Gaussian, which we call AssymWidth. The energy of the SNE is given as a fraction of the gravitational binding energy of the star. We call this fraction SNEfrac. For example, an explosion with SNEfrac = 0.2 means that the kinetic energy of the SNE equals 20% of the gravitational binding energy of the pre-supernova stellar model.

We run these initial conditions for different values of SNEfrac. Five scenarios of SNEfrac are tested: 0.2, 0.4, 0.6, 0.8 and 0.9. The asymmetry is adjusted so that, by conservation of linear momentum, the initial BH speed is either 200km/s, 500km/s, 1000km/s or 1500km/s. We call these speeds the initial kick of the compact object. This range of NKs were chosen taking into account Fig. 2.4. Because almost all NK possibilities are in a range of 1000km/s or less, 1000km/s is taken as a maximum for observable NS NKs. 1500km/s is an unrealistic scenario that we construct to study a wide range of NKs and to determine how high the NK must be in order to change the direction of the orbital system. The idea behind this is to study the final speed of the BH after the accretion of fallback material. We call the BH kick after accretion the final kick of the BH. These initial conditions are ran for 2 solar dynamical times (around 3200s), and we study the resulting speed and mass of the BH after accretion. The reasoning is that, at the beginning of the SNE, the distribution of kicks should be reminiscent of what is observed for NS, but the BH kicks should take into account the additional mass accreted. With this setup it is possible to determine whether the BH kicks are scaled by the factor expected from spherically symmetric accretion, or not.

After studying the initial conditions mentioned in the last paragraph, we can then add a BBH with a slightly higher mass than the pre-supernova stellar model, in order to make a BBH system consistent with Fig 2.1. In order to avoid the disruption of the BBH system, and to make the best case scenario for the possibility of producing a negative χ_{eff}, the kick is added in the orbital plane, and opposite to the initial orbital speed (see Section 2.2). The initial separation of the binary is wide enough so that tidal locking is not a possibility, and close enough so that they will merge before the Hubble time. For instance, the $28M_{\odot}$ will have a binary BH with $30M_{\odot}$ and an initial separation of $40R_{\odot}$. These systems begin with 0 eccentricity because we expect these systems to be close to circular before the second SNE, but they may gain eccentricity after the NK. Everything else regarding the initial conditions of this binary system is done the same way as mentioned before. We add to the binary system an initial NK of 1000km/s, to further study a realistic best-case scenario.

3.4 Convergence tests

Most of the convergence tests where done for the $28M_{\odot}$ stellar model. We ran simulations following the initial conditions and methodology described in section 3.3. We ran simulations with a number of SPH particles ranging from 10^6 to 10^7. For the case of $N = 2 \times 10^6$ and $N = 4 \times 10^6$, two simulations were run to make sure that the randomness regarding the particle distribution along the star does not have a significant effect on the final results. Fig 3.3 and Fig 3.4 show the results obtained.

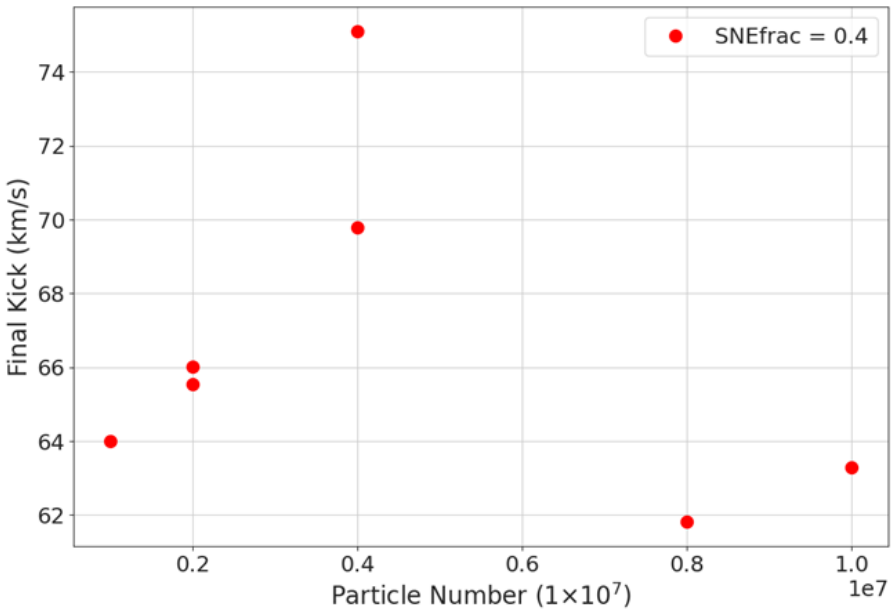

Figure 3.3: Final velocity of the BH after accretion, as a function of the number of SPH particles. Each point in the graph represents a different simulation. The BH had an initial NK of 400 km/s. The simulation corresponds to the pre-supernova stellar model of $28M_{\odot}$.

Regarding Fig 3.3, it is important to mention that, for the purposes of obtaining χ_{eff}, a difference between a final NK of 15 km/s, or even 30 km/s is not at all significant. Fig 3.3 shows final NKs that range from 61.8 km/s to at most 75.1 km/s. This difference is not relevant for our research.

Fig 3.4 shows quite an interesting result. We consistently found, throughout multiple runs, a significant reduction of the final mass of the BH after accretion, when the range of number of SPH particles goes from $N = 10^6$ to $N = 10^7$. After $N = 8 \times 10^6$, the difference in the final BH mass if one increases the number of SPH particles stops being relevant. We believe this effect is due to the fact that, for a small number of SPH particles, each individual particle is much more massive, and each time the BH consumes a particle in the simulation, the amount of mass that the BH gains is larger

than with a higher resolution.

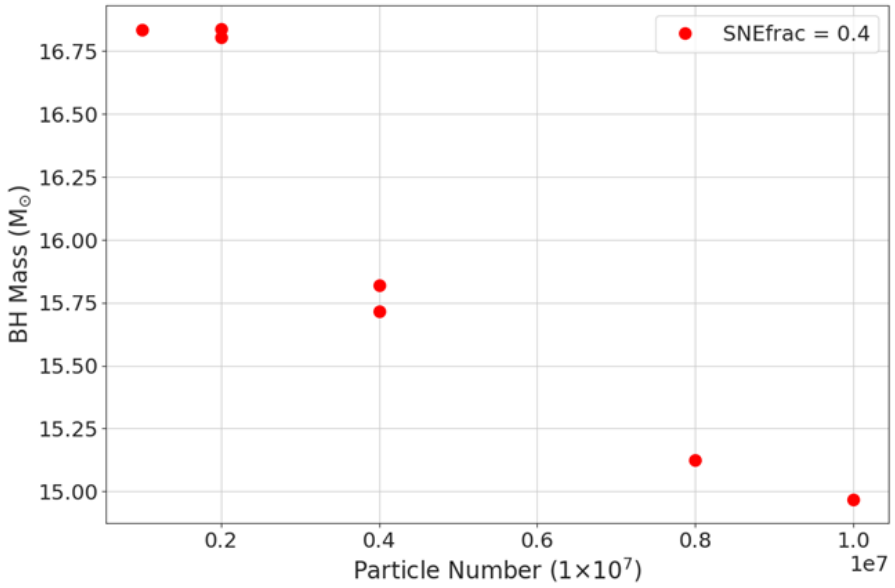

Figure 3.4: Final mass of the BH after accretion, as a function of the number of SPH particles. Each point in the graph represents a different simulation. The BH had an initial NK of 400 km/s. The simulation corresponds to the pre-supernova stellar model of $28M_{\odot}$.

Based on this results, we conclude that running simulations with $N = 1 \times 10^6$ works for making calculations regarding the final NK of the BH after accretion, having in mind that calculations that include the final mass of the system may be overestimated. For simulations where we require a higher certainty in the final mass, running simulations with $N = 8 \times 10^6$ works better.

To make sure that everything was consistent in the $21M_{\odot}$ stellar model, we ran some convergence tests with this model as well. We ran fewer tests, and the results are still consistent with what was previously mentioned. Both the convergent tests and all the results of the $21M_{\odot}$ star can be found in the Appendix A.

Chapter 4

Results

4.1 Properties of the Black Hole after accretion

We begin by studying the simulations with an isolated BH in the range of SNE energies and initial kicks mentioned in Section 3.3.2. Since these simulations do not include the binary companion, when studying the properties of the binary system, we will obtain the results using the formulation presented in Section 2.2.1, by assuming an instantaneous loss of mass. We can then compare these results with the simulations ran with the binary system. In this chapter, the results for the $28M_{\odot}$ star will be presented. The results for the $21M_{\odot}$ star are presented in the Appendix A. As mentioned in the last section, the $28M_{\odot}$ star is assumed to have a binary companion of $30M_{\odot}$ and an initial orbital separation of $40R_{\odot}$. In total, this section presents the results of 20 different simulations.

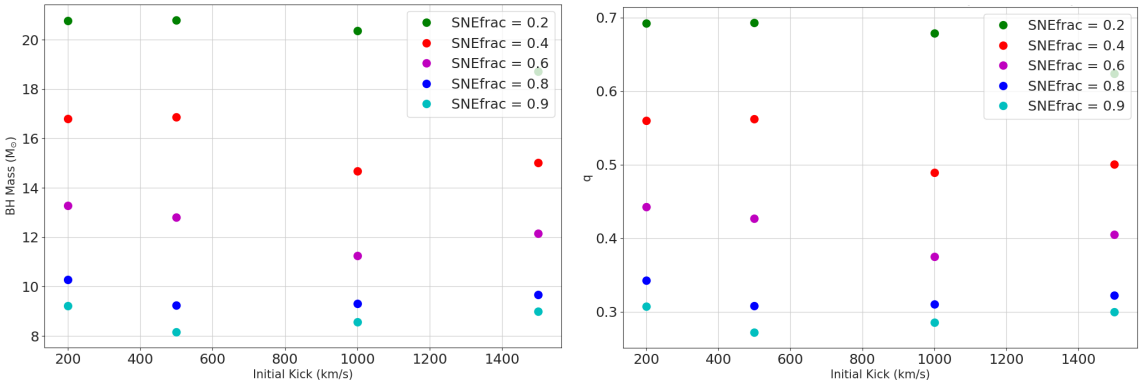

Figure 4.1: **Left:** Final mass of the BH after accretion vs the initial NK. **Right:** Final mass fraction of the binary system after accretion, assuming a secondary star of $30M_{\odot}$.

Fig. 4.1 shows the final mass of the BH after accretion, for the different SNE

energies and initial kicks. As expected, a lower energy SNE will allow the BH to accrete more mass, and thus it ends with higher masses than those with higher SNE energies. Regarding the figure from the right, it is important to mention that, as was explained in Section 1.2.1, most sources seem to have similar masses, but it is also possible to find systems with relatively low ratios of masses. It is easy to see from Fig. 4.1 that a high energy SNE will result in systems of less similar masses, which is something important to take into account when analyzing the observations, if this were in fact the formation mechanism at play in this systems.

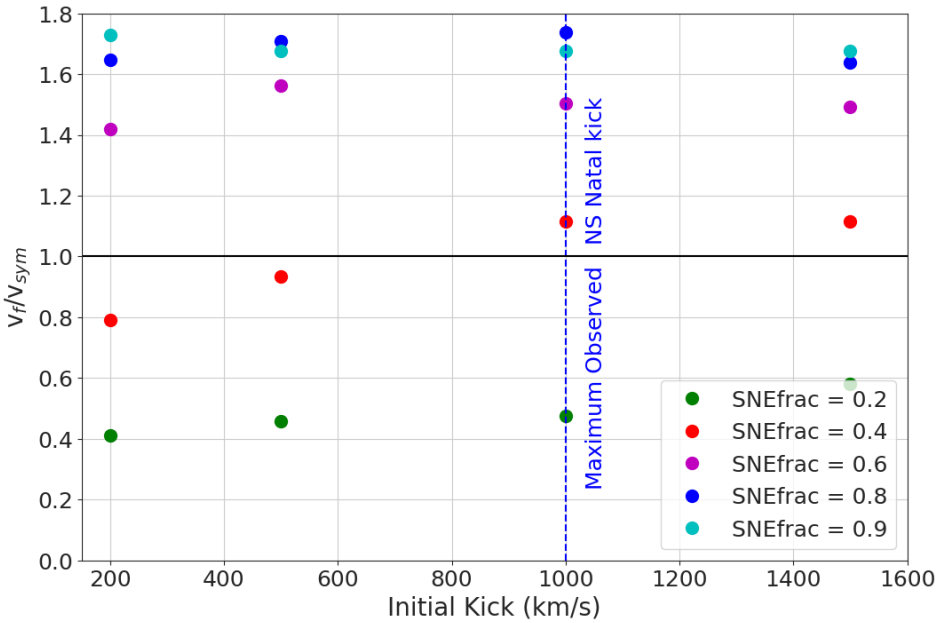

Figure 4.2: Fraction between final BH speed and speed expected from accretion vs initial BH speed, for different explosion energies, with $N_{SPH} = 10^6$. The simulation corresponds to the pre-supernova stellar model of $28M_{\odot}$.

Fig. 4.2 shows the fraction between the final BH speed after accretion, and the value expected with symmetric accretion ($v_{\rm sym} = (m_i/m_f)v_i$). Our results indicate that the final speed of the BH after accretion is either lower than $v_{\rm sym}$, close to $v_{\rm sym}$, or larger, depending on the energy of the explosion. Fig. 4.2 also shows that increasing the SNE energies increase the final speeds compared with symmetrical accretion, up to a limit. Adding additional energy to the explosion does not increase arbitrarily the $v_f/v_{\rm sym}$ fraction. We ran additional test simulations for higher SNEfracs and we did not manage to obtain fractions greater than 1.8. What we can definitively say, is that variations in the SNE energy and in the asymmetry yields different values for $v_f/v_{\rm sym}$, which suggests that a mechanism like the one presented by Janka 2013 may be at play [18]. We can also say, that the scenario for the expected distribution of BH NKs

is more complicated than just scaling the NS NKs by the ratio of masses.

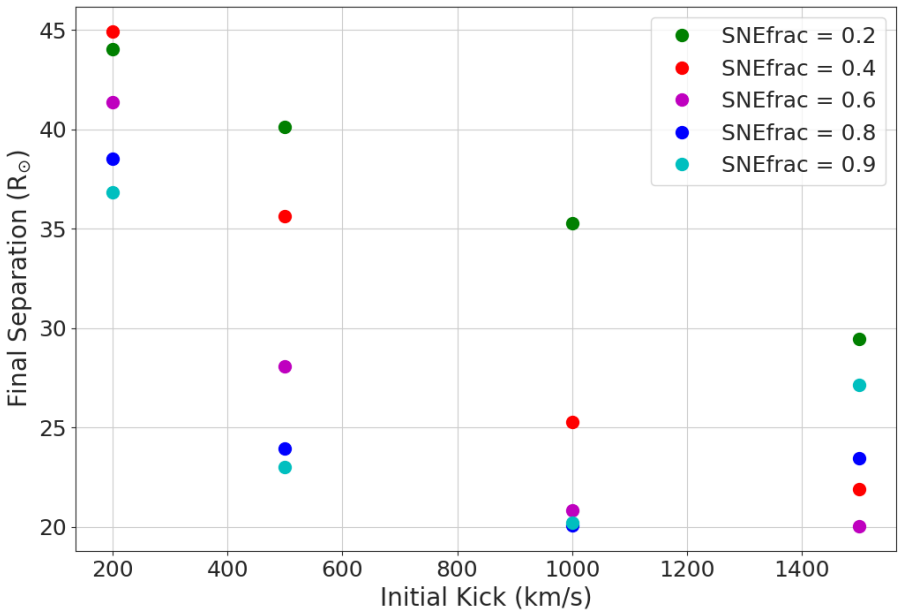

Figure 4.3: Calculated final separation, assuming instantaneous mass loss, vs initial BH speed, for different explosion energies, with $N_{SPH} = 10^6$. The simulation corresponds to the pre-supernova stellar model of $28M_\odot$. The calculations are based on Brandt & Podsialowski 1995, assuming a secondary star of $30M_\odot$ and an initial separation of $40R_\odot$. [9]

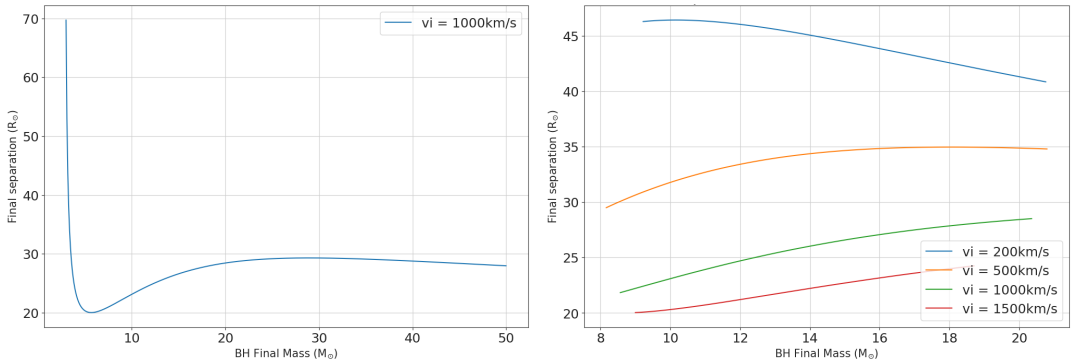

Figure 4.4: **Left:** Final separation as a function of the final mass of the BH, assuming spherically symmetric accretion and an initial kick of 1000km/s. **Right:** Final separations as a function of the final mass of the BH, assuming spherically symmetric accretion. The calculations for both figures are based on Brandt & Podsialowski 1995, assuming a secondary star of $30M_\odot$ and an initial separation of $40R_\odot$. [9]

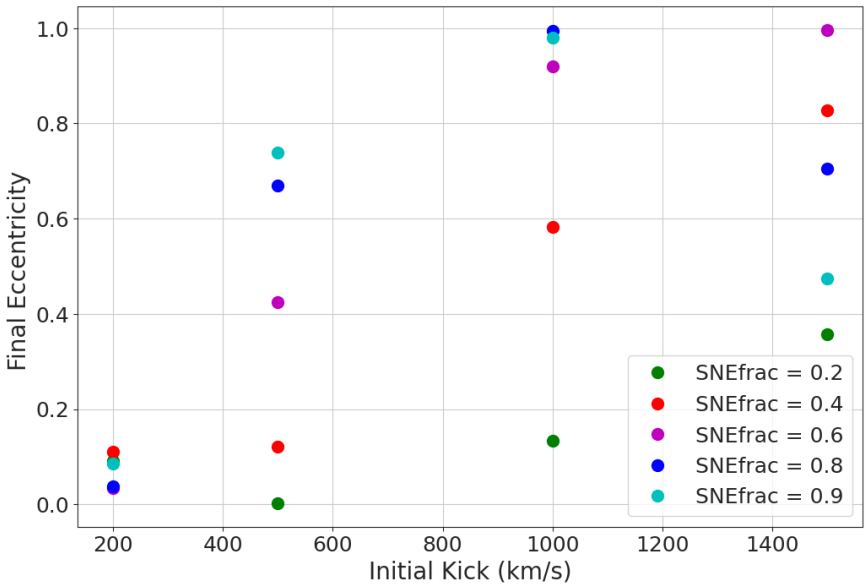

Figure 4.5: Calculated final eccentricity, assuming instantaneous mass loss, vs initial BH speed, for different explosion energies, with $N_{SPH} = 10^6$. The simulation corresponds to the pre-supernova stellar model of $28M_\odot$. The calculations are based on Brandt & Podsialowski 1995, assuming a secondary star of $30M_\odot$. [9]

Fig 4.3 shows the final separation of a binary system comprised of the simulated BH and a $30M_\odot$ companion. This calculations are done assuming an instantaneous loss of mass, but they will be compared with simulations of the binary systems. It is in our interest to study how accurate the instantaneous loss of mass approximation is, which is the reason why it is important to make the comparison. To make the calculations, the kick is assumed to be in the orbital plane and opposite to the initial orbital speed. This is done because that is how the kick was defined in the simulations with the binary companion, so we want the comparison of the simulations to be analogous between them. As mentioned in Section 3.3.2, this direction for the NK is the best case scenario, to allow the NK to produce a negative χ_{eff} without disrupting the binary. It is interesting to note that higher initial kicks yield smaller final separations and higher eccentricities of the system for SNEfracs of 0.2, 0.4 and 0.6. For SNEfracs of 0.8 and 0.9, the initial kick of 1000km/s yields the smallest separation and the highest eccentricity. We will explain the final separation and the eccentricity with different arguments.

The complex nature of the final separation is explained by considering the equation (2.7). Both $\tilde{m}$ and $\tilde{v}$ depend on the mass of the system after accretion. The case of $\tilde{m}$ is by definition (see eq. (2.4)), and in the case of $\tilde{v}$, it is correlated with the mass after accretion because the final kick of the simulation depends on the SNE energy, and the final BH mass depends on the SNE energy as well. In fact, if one were to use v_{sym} (see eq. (1.1)), then the kick velocity after accretion would depend directly on the initial

kick, and the mass of the BH after accretion,

$$a' = \frac{a}{2 - \frac{M_i + M_2}{M_f + M_2}\left[1 - \frac{M_i}{M_f}\frac{v_i}{v_{orb}}\right]^2}. \tag{4.1}$$

This means that there is a complicated relationship between the initial kick and the final separation of the system. Fig. 4.4 calculates the final separation as a function of only two parameters: The initial kick and the BH final mass, by using Eq. (4.1). This was done by assuming spherically symmetric accretion because, otherwise, the final kick would be an additional parameter. The left figure shows a wide range of masses over one particular initial kick to show the general shape of the curve, and the right figure shows how different initial kicks and masses can take on different parts of the curve of the left. Because the general curve shifts to the left or to the right when changing the initial kick, they experience different parts of the curve. By comparing with Fig. 4.3, one can say that the SNEfracs of 0.2, 0.4 and 0.6 are taking the strictly decreasing part of the curve, whereas the SNEfracs of 0.8 and 0.9 take the part of the curve that decreases and then increases, which makes sense considering that this part happens for smaller masses, which are the ones obtained from higher energies.

The behaviour in Fig. 4.4 Right cannot be exactly mapped onto Fig. 4.3 because the $v_{\rm sym}$ would need to be multiplied by a factor depending on the energy of the explosion, as can be observed from Fig. 4.2. This factor would be different for different values of the BH final mass, and this also changes the behavior of the graph. Something interesting that can be said, is that, on average, higher separations in Fig. 4.3 correspond to lower eccentricities in Fig. 4.5, and the other way around.

Fig. 4.5 shows the relationship between the initial kick and the final eccentricity, by assuming an instantaneous loss of mass. Lets consider the orbital system we are working with. A binary system of two initial masses of $28M_\odot$ and $30M_\odot$ respectively, with an initial separation of $40R_\odot$, will have an initial orbital speed of ~ 600km/s. If the NK after accretion exceeds the orbital velocity, the BH will change direction relative to a rest frame, and its angular momentum will change sign. The simulations that resulted in lower separations and higher eccentricities coincide with the simulations with a final kick after accretion near the orbital speed of the system. This makes sense because the angular momentum in these systems will diminish significantly because the BH stops relative to a rest frame. A lower angular momentum means a smaller periastron, and a higher eccentricity if taken into account that the initial separation of all simulations is the same. With this in mind, it is reasonable to say that, because NKs of 1000km/s and 1500km/s are more likely to have final kicks closer to the orbital speed after accretion,

this will result in closer and more eccentric systems, once the orbit stabilizes.

There were a couple of systems with eccentricities very close to 1, so it is reasonable to wonder whether these systems are still bounded. We calculated the orbital energies of these systems to make sure that they are still bounded, and they are. Even though these extreme systems are still in orbit, the semi-minor axis of them are in the order of $\sim 0.1 R_\odot$. This will be important when studying the time of merger of the systems.

Fig. 4.6 shows both the behavior of the maximum possible separation allowed for a system of a certain mass to merge in the age of the Universe vs the eccentricity of the system in the left figure, and the fraction between the final separation shown in Fig. 4.3, and the maximum separation (a_f/a_{max}) in the right figure. In the left figure, the dots represent the actual final separations of the simulations, so that they can be compared with the maximum separations.

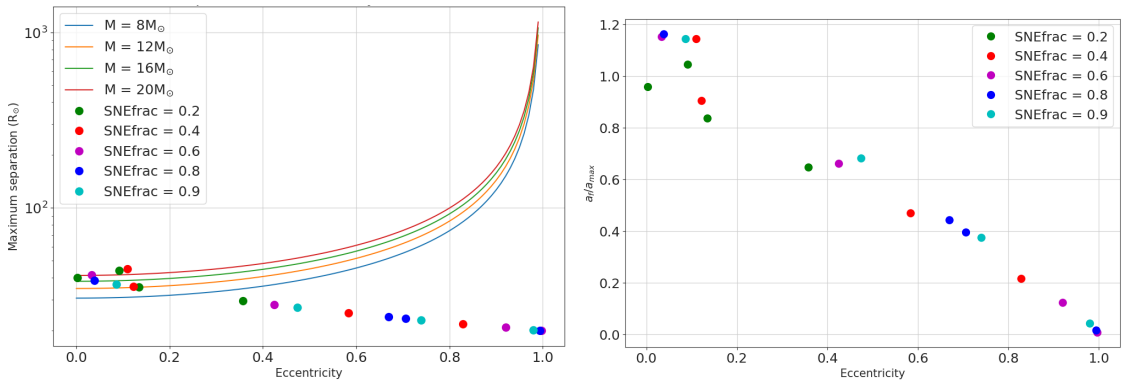

Figure 4.6: **Left:** Maximum separation allowed for a binary system to be observed through GWs, as a function of the eccentricity after the NK. The solid lines represents how the maximum separation changes with eccentricity for different masses. The dots represent the final separation in the simulations. **Right:** Fraction between the final separation and the maximum separation allowed for a binary system to be observed through GWs, as a function of the Final eccentricity of the orbit. The calculations for the final separation and eccentricity are based on Brandt & Podsialowski 1995, assuming a secondary star of $30 M_\odot$ and an initial separation of $40 R_\odot$. [9]. The maximum separation is calculated based on the review of Postnov & Yungelson 2014 [26].

It is possible to see that the systems with lower eccentricities (which had bigger separations after accretion) show dots above some solid lines. However, it is not clear which final masses those simulation have, to know to which solid lines to make the comparison. The right plot of Fig. 4.6 shows the fraction of each individual final separation with the maximum separation for a system of their given masses and eccentricity. Systems with ($a_f/a_{max} > 1$) are not observable. However, this is not an issue for our objectives, because we are interested in systems with high enough NKs to change the

sign of the angular momentum. As Fig. 4.5 shows, this low eccentricity systems are also the ones with initial kicks smaller than the orbital speed, which makes them highly unlikely as candidates for having a negative χ_{eff}. As a final remark, it is unsurprising that some systems were not going to be observable because we gave an initial separation close to the limit of what can merge before the age of the Universe, because we want the orbital speed to be as low as reasonably possible to make it easier for the NKs to change the direction of the orbit.

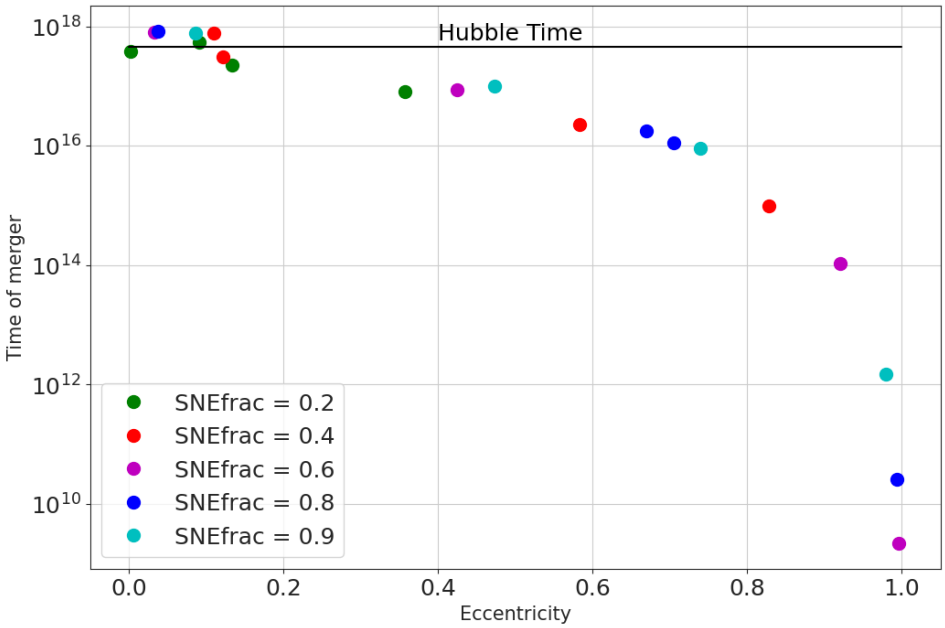

Figure 4.7: Calculated time of merger for the BBH, vs eccentricity, for different explosion energies, with $N_{SPH} = 10^6$. The solid black line corresponds to the Hubble time.

It is also important to notice the exponential nature of the maximum observable separation of the system, and its eccentricity. This behavior can also be observed in Fig. 4.7, which shows the relationship between the merger time of the simulations, and their eccentricities. It is well known that the GWs are more prevalent the closer the masses are between them. More eccentric orbits have a smaller periastron, which allows the BHs to get closer between them and emit more GWs. Thus, higher eccentric systems merge faster [26]. It is clear that, if a higher eccentricity helps the binary system merge in less time, then the maximum separation allowed is bigger than the a_{max} for less eccentric systems, which is the reason why the exponential function in Fig. 4.3 is increasing, but in Fig. 4.5 it is decreasing.

The systems that are more likely to change the angular momentum of the binary system are the ones with initial kicks of 1000km/s and 1500km/s. This can be concluded from this section because those are the ones which, after accretion, have some systems

with final kicks greater than the orbital speed. This does not necessarily guarantee that these initial kicks can change the angular momentum, because it is also important for the kick to be directed on the right direction, which does not happen always. We can also conclude from this section that, if the kick is in the right direction, we should not worry that high velocity NKs will disrupt the binary to the point that they would not be bounded, or to the point that they would not merge on time.

4.2 Properties of the binary system

In this section, we will study simulations made with the binary system. These simulations we done with a number of SPH particles of $N_{SPH} = 8 \times 10^6$, a $30M_\odot$ BH companion and $40R_\odot$ of initial separation. Because $N_{SPH} = 8 \times 10^6$ simulations are more time consuming for the supercomputer, we were conservative in the amount of simulations necessary to draw our conclusions. The simulations in the last section were done with $N_{SPH} = 1 \times 10^6$. These simulations, besides helping us test the accuracy (or lack thereof) of assuming spherically symmetric accretion in analytic calculations, allowed us to map the space of possibilities for these systems, which helped us decide better which initial conditions we wanted to test further. As mentioned at the end of the last section, it is now clear that, even though the majority of initial NKs are smaller than 1000km/s, these systems are the ones that are more likely to change the direction of the orbit of the binary system. Even though the initial NKs of 1500km/s are also likely candidates to change the direction of the orbit, no kick of this magnitude has been observed. For this reason, in this section we will focus on initial kicks of 1000km/s, and the same ranges of SNE energies (SNEfracs of 0.2, 0.4, 0.6, 0.8 and 0.9).

Fig 4.8 compare the fraction between the final separation of the binary and the final separation of the isolated simulation vs time. It is important to mention that the more energy a SNE explosion has, the quicker this explosion will occur, and a result of this is that the instantaneous mass loss approximation should apply better.

Because the SNEfracs of 0.8 and 0.9 correspond to the quickest explosions, they would also be the best approximations of the instantaneous mass loss case in our simulations. Because of this, it stands to reason that these simulations should return closer values to the ones calculated with Eq. (2.7). It is clear from the figure that the simulations with final values closer to 1 (meaning that the calculations describe accurately the simulations) match with the systems of greater SNE energy. The simulations with SNEfracs of 0.2, 0.4 and 0.6 show discrepancies with the calculations, meaning that it would not be reasonable to utilize the instantaneous mass loss approximations in

those cases. Fig. 4.9 shows similar results to those in Fig. 4.8 but with eccentricity instead of final separation. Here, the pattern between SNEfrac and the accuracy of the instantaneous mass loss approximation is much more clear. It is possible to observe how the bigger the SNE explosion, the closer the fraction approaches one.

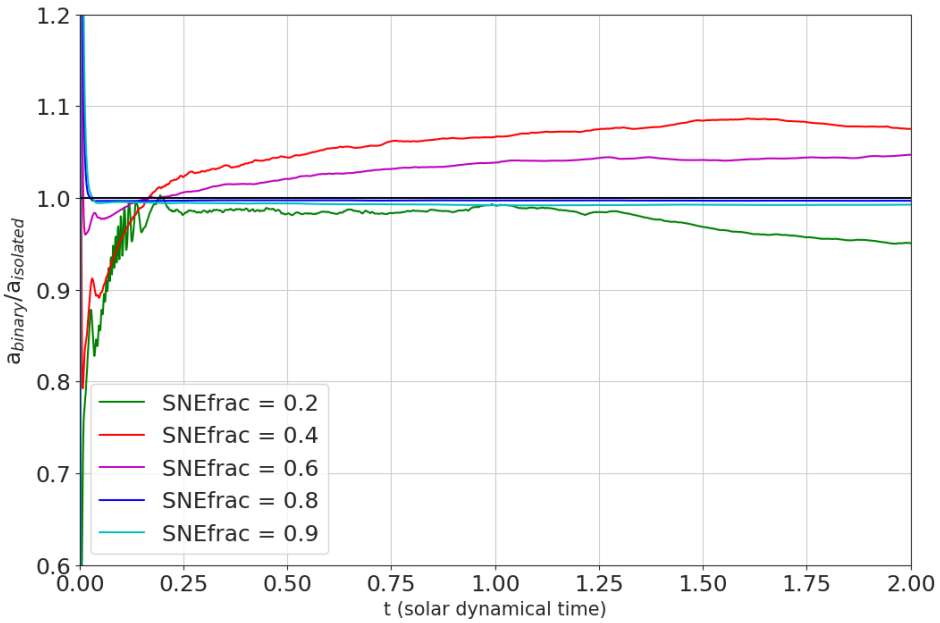

Figure 4.8: Final separation of the Binary system as a fraction of the calculation assuming instantaneous mass loss, vs time, for different explosion energies, with $N_{SPH} = 8 \times 10^6$. The simulations correspond to the pre-supernova stellar model of $28M_\odot$, a secondary star of $30M_\odot$, and an initial BH speed of 1000 km/s.

Fig. 4.10 shows the L_z of the system, relative to the center of mass, for different SNEfracs. Notice how, because we are working with initial NKs of 1000km/s in opposite direction to the orbital speed of the orbit, all L_z's initiate as negative. Over time, once the BH accretes mass, the final BH kick, and its relationship with the orbital speed of the system (which is $\sim$ 600km/s), is what defines whether the orbital angular momentum will change sign or not.

It is clear that SNEfracs of 0.2, 0.4 and 0.6 give a positive angular momentum, a SNEfrac of 0.8 give L_zs consistent with zero, and an SNEfrac of 0.9 does achieve to keep the angular momentum in the negatives. Let us remember for a moment that most NKs have a speed of 500km/s or less. In this section, we are working with initial NKs of 1000km/s, which are at the limit of what has been observed, and still the majority of cases studied do not manage to turn around the orbit. It seems that only a set of very specific initial conditions allow for a negative L_z.

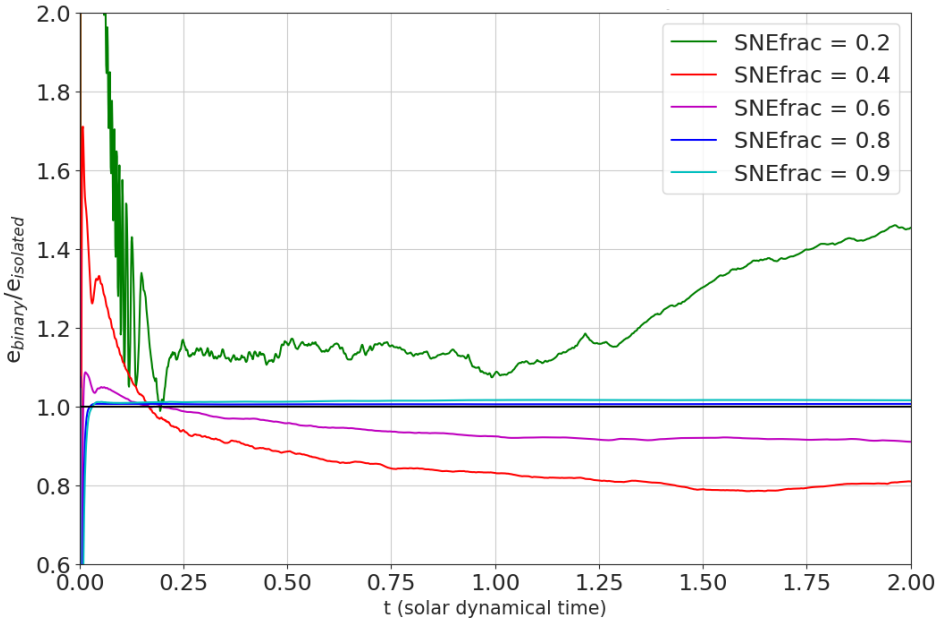

Figure 4.9: Final eccentricity of the binary system as a fraction of the calculation assuming instantaneous mass loss, vs time, for different explosion energies, with $N_{SPH} = 8 \times 10^6$. The simulations correspond to the pre-supernova stellar model of $28M_\odot$, a secondary star of $30M_\odot$, and an initial BH speed of 1000 km/s.

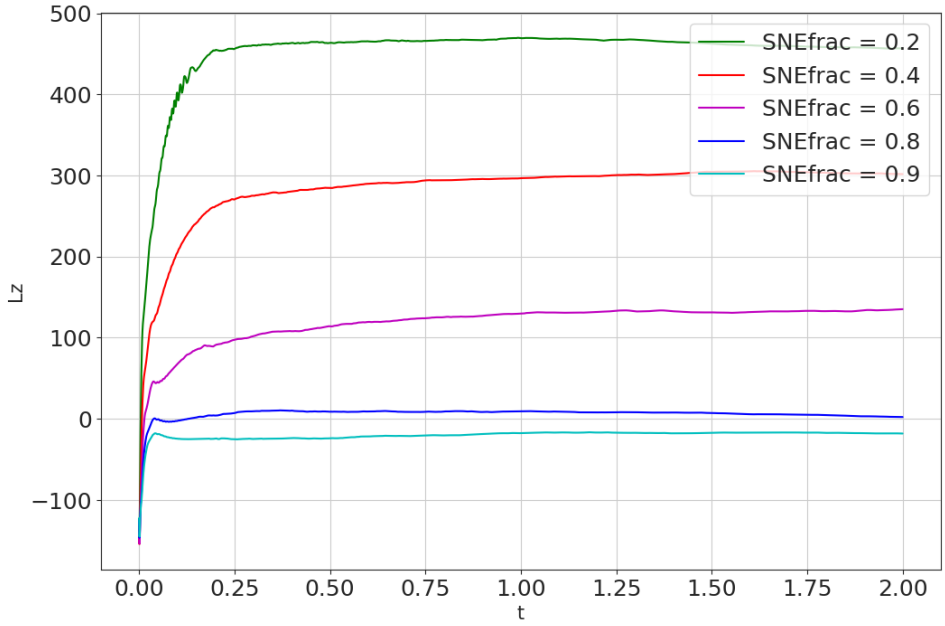

Figure 4.10: Angular momentum in the z axis vs time (measured from the center of mass) of the relative orbit, for a BH formed from a $28M_\odot$ star with a $30M_\odot$ companion and different explosion energies with $N_{SPH} = 8 \times 10^6$.

Fig. 4.11 shows the dimensionless spin parameter perpendicular to the orbit of the second-born BH, as a function of time. it is clear from the values at play in this figure,

that the dimensionless spin parameter of the second-born BH in our simulations is consistent with 0. The spin changes without following a clear pattern. We do expect the value of the spin to change by accretion of material. What is really interesting is that some of the simulations ended with negative final values (although still consistent with 0) for the final spin of the BH. This is due to the asymmetrical accretion of material, which makes the amount of angular momentum accreted less predictable. It is possible that this is another mechanism that could potentially result in a negative value for χ_{eff}, although it is unlikely that this mechanism would play out in an initially rapid-rotating BH. Future research should look into this potential mechanism. That said, it is also important to notice that these simulations that ended with a negative value for χ_{1z}, did not result in negative values for χ_{eff}. The spin of the first-born BH would also be an important factor at play here.

Fig 4.12 shows the calculated effective spin parameter of the binary system vs time, assuming that the companion has a dimensionless spin parameter of either 0.1 or 0.2. We mentioned in Section 2.1.1 that it is expected for the first-born BH to have low spins due to the fact that they give most of their angular momentum to the companion in the mass transfer. For this reason, we see 0.1 and 0.2 as relatively high spins for this BH.

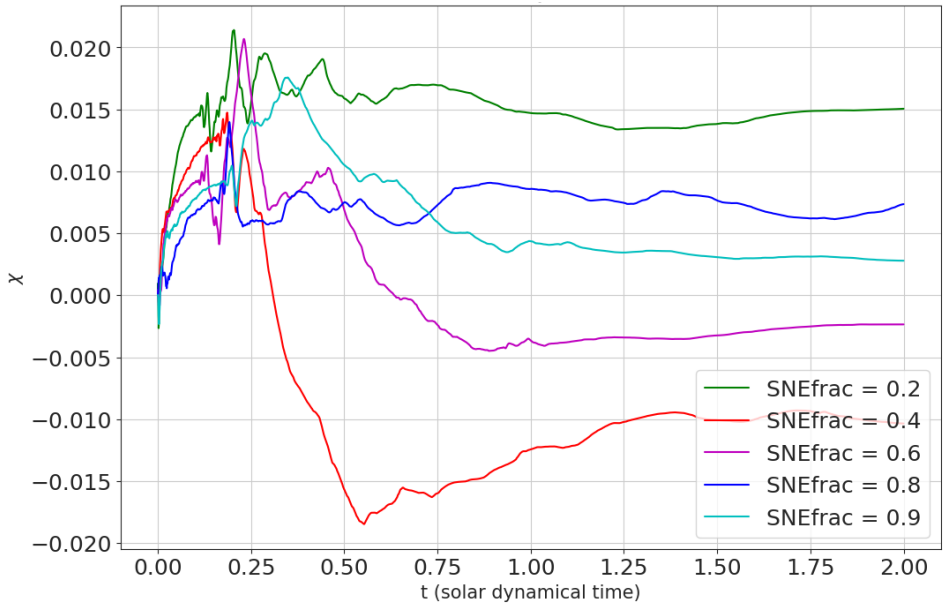

Figure 4.11: Individual spin vs time, for a BH formed from a $28M_{\odot}$ star and different explosion energies with $N_{\text{SPH}} = 8 \times 10^6$.

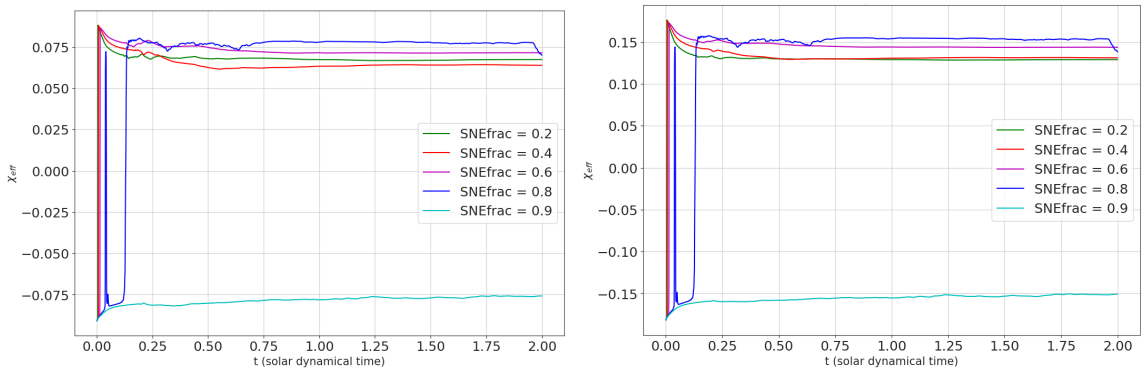

Figure 4.12: **Left:** Effective spin parameter of the binary system as a function of time, assuming the $30M_{\odot}$ has an individual spin of $\chi_2 = 0.1$. **Right:** Effective spin parameter of the binary system as a function of time, assuming the $30M_{\odot}$ has an individual spin of $\chi_2 = 0.2$.

In a similar fashion to Fig. 4.10, notice how, because we are dealing with initial kicks of 1000km/s, all simulation begin with a negative effective spin. once the accretion stops, all but the SNEfrac=0.9 simulation stabilizes in positive values. It should not be surprising that the SNEfrac=0.8 simulation jumps a bit between being positive or negative, if one notices that this is also the case for its L_z in Fig. 4.10. It is also interesting to notice that, in the end of the SNEfrac=0.8 simulation, the effective spin parameter decreases, as the value for the L_z of the system approaches 0. It is unclear whether the final χ_{eff} would have stabilized in a positive of negative value, if the simulation were ran for longer. However, it is reasonable to conclude that lower SNEfracs are likely to lead to positive values of χ_{eff}, and higher SNEfracs would give negative values.

Notice that even though the L_z changes drastically from one simulation to another, the values for χ_{eff} do not change as much. This is because the absolute value of χ_{eff} is defined by the individual spins of the BHs. The orbital angular momentum will only tell us the sign of the effective spin parameter. This is why in Fig. 4.12 the absolute value changes drastically when χ_2 changes from 0.1 to 0.2. χ_2 is determinant in the absolute value (not the sign) of the effective spin parameter, because the dimensionless spin parameter of the BH formed in the simulated SNE is very low. As mentioned in Section 3.3.1, future research can include simulations with higher initial rotations of the star, although we do not expect these additional simulations to change significantly the answer to question of whether NKs can consistently change the sign of the effective spin parameter, because this would mainly occur by flipping the direction of the orbit (the sign of L_z). .

Finally, Fig. 4.13 shows the preccesion spin parameter vs time. Having into account

that this parameter is positive by definition, it does not appear to have any clear pattern as well. The amount this parameter increases (or decreases) would be determined by the amount of angular momentum in the x and y axis that would be accreted by the BH during the SNE. Among all simulations, the initial L_x and L_y of the entire star was around 100 times less than L_z. This initial values were done to the randomness of the initial conditions construction, explained in Section 3.3.2.

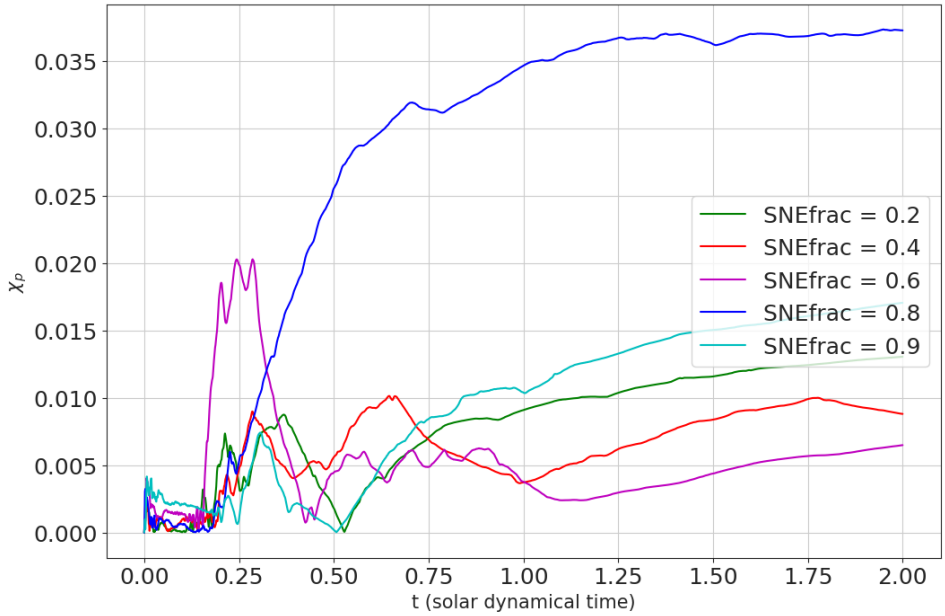

Figure 4.13: Precession spin parameter vs time, for a BH formed from a $28M_\odot$ star with a $30M_\odot$ companion and different explosion energies with $N_{SPH} = 8 \times 10^6$.

Chapter 5

Summary and Conclusions

Since the discovery of GWs, it has been very important to understand the formation mechanisms behind the BBHs that the LVK collaboration is capable of detecting. Depending on the formation channel of the BBH, different possible distributions of χ_{eff} are expected [31]. For BBHs that are created from dynamical interactions in dense stellar environments, we expect a random distribution of χ_{eff} between -1 and 1. This is due to the numerous interactions the BBHs would be experiencing in this environment [8, 23]. Another mechanism for the formation of BBHs would be isolated stellar binary systems. From these systems, one would expect the individual spins of the binary components to be aligned with the orbital angular momentum. This would mean that, from isolated stellar binary systems, one would initially expect a positive distribution of values for χ_{eff}, unless there is another mechanism at play [23, 31].

It has been proposed that a BH NK of linear momentum can be theoretically able to change the direction of the orbit, and as a result, the sign of χ_{eff}. This NK can be the result of an asymmetric SNE [9, 18]. If the integrated momentum of the SNE tends towards a particular direction, the compact object would go to the opposite direction to conserve linear momentum. These NKs have been observed numerous times in NSs, but NK detections in BHs are still limited. [30]

Theoretical calculations have been made to calculate how should the distribution of BH NKs be, and how big the NK should be to change the sign of χ_{eff}. In particular, Janka (2013) proposed that the BH NKs should be bigger than the reduced NKs of Neutron Stars after a spherically symmetric accretion of mass and momentum In the simplest scenario one would expect that the NK received by the NS that eventually collapses into a BH would be reduced by the accretion process. However, Janka proposes that the BH NK would be bigger, by means of a gravitational tug boat mechanism [18].

However, the analytic calculations on BH natal kicks using eq.(1.1) do not follow

the entire evolution of the accretion of mass and momentum from the asymmetric SNE ejecta. In order to study this scenario we analyzed the process of accretion of material by a newly formed BH located in the center of an exploding star, whose NK will be determined by the asymmetry of the explosion. This was done by means of 3D SPH simulations of pre-supernova stellar models with $21M_{\odot}$ and $28M_{\odot}$. This would allow us to follow the process of accretion, and the entire evolution of the BH's properties (including the NK). Our objective from this work is to answer if the resulting BH NK after accretion would suffice to consistently change the sign of $\chi_{\rm eff}$.

To construct the initial conditions, the pre-supernova stellar models were taken from the work of Woosley & Heger 2006. We chose stars consistent with the range of observations from GWs, but we focus on the $28M_{\odot}$ to show the results. The results for the $21M_{\odot}$ can be obtained in the Appendix A. From these stellar models, the SPH particles were located in proportionality to the density of the star at each radius. The particles were given the initial rotation of the star. The first $3M_{\odot}$ from the center of the star outwards, was reduced to a single sink particle which corresponds to the BH. Then, the next solar mass outwards was given the kinetic energy of the explosion, with an asymmetry taken into account to produce a NK. The speed necessary the BH would need to conserve the initial momentum before the SNE would be given to the BH.

From our convergence tests, we concluded that we could begin with simulations of the isolated asymmetric SNEs that use 1×10^6 SPH particles to test the space of possibilities, and to see how accurate the spherically symmetric accretion approximation is. A wide range of NKs was simulated by changing the amount of asymmetry in the explosion. There was also variation in the SNE energies, given as percentages of the gravitational binding energy of the star. We calculated the hypothetical final separation and eccentricity of a system comprising our simulated star and a companion with slightly higher mass, and a separation in the limit of what would be observable with GWs. Additionally, the time of merger and maximum final separations allowed for the systems to be observable were analyzed.

After running these simulations and analyzing the results, additional simulations of a binary system were ran with 8×10^6 SPH particles, for the $28M_{\odot}$ star with a first-born BH of $30M_{\odot}$ and an initial separation of $40R_{\odot}$. We calculated the separation and eccentricity of the system to compare with the ones calculated previously and to test the instantaneous loss of mass approximation. We also calculated the angular momentum measured from the center of mass and the effective spin parameter of the binary, assuming certain values for the spin of the first-born BH. Finally, the individual spin of the second-born BH and the precession spin parameter was analyzed.

Our conclusions are as follows:

1. Higher energies of the explosion will result in BBHs with unequal masses. Most observations are consistent with mass fractions closer to 1, but systems with unequal masses have been observed before.

2. The final speed of the BH after accretion can be lower, equal, or larger than the one expected from spherically symmetric accretion ($v_{\rm sym}$), depending on the energy of the explosion. SNEs with an energy of 20% of the gravitational binding energy of the star gave consistently lower values than $v_{\rm sym}$, whereas SNEs with a percentage of 60% or more gave final speeds higher than $v_{\rm sym}$. This indicates that the mechanism described by Janka 2013 may be at play [18].

3. Whether a gravitational tug boat mechanism does happen or not, it is undeniable that the asymmetrical accretion must be taken into account because it significantly alters the result of the final speed of the BH after accretion. The amount of the alteration depends on the SNE energy.

4. The final separation and eccentricity of these systems with high velocity NKs are indeed observable by GWs, mainly due to the fact that they end up with eccentricities that help them merge before the Hubble time. Some of our simulations with NKs of 200km/s had final separations larger than the maximum allowed for them to be observable, but this aren't the types of systems that would change the orientation of the orbit regardless.

5. Even though the final separation of the binary systems changes by no more than 10% from the calculations done by assuming an instantaneous loss of mass in the SNE, the eccentricities have bigger changes than the ones calculated. Explosions with energies of around 80% the gravitational binding energy of the star of higher gave results very similar to the calculations, which means that the instantaneous loss of mass is a good approximation in those cases.

6. Even NKs of $\sim$ 1000km/s, which are among the highest speeds observed for NS, were not able to consistently change the orientation of the orbit, thus returning a negative value of $\chi_{\rm eff}$. The best case scenario for negative $\chi_{\rm eff}$, which are systems with high observable initial separations, and a kick perfectly directed against the orbital speeds, only change the orientation of the orbit in the simulation with SNE energy of 90% the gravitational binding energy of the star.

7. The individual spin of the second-born BH and the precession spin parameter does changes during the accretion process without following a specific pattern. We found that it is possible for the individual spin to change sign by means of the asymmetrical accretion, provided that the initial angular momentum of the BH is low to begin with. This can possibly be another mechanism to change the sign of χ_{eff}, but additional research should be done to test this hypothesis, and it is unlikely for this scenario to happen with higher rotating BHs.

Appendix

Appendix A

Results for the 21$M_\odot$ star

A.1 Convergence tests

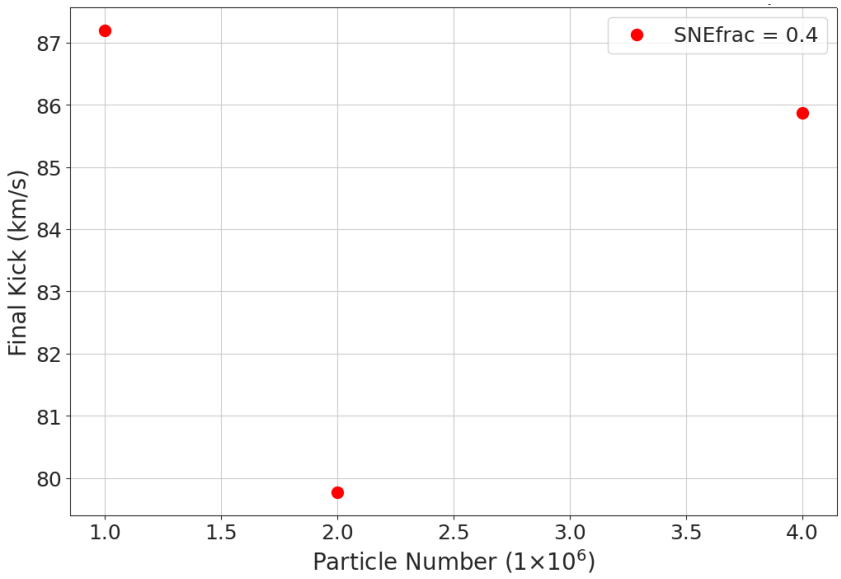

Figure A.1: Final velocity of the BH after accretion, as a function of the number of SPH particles. Each point in the graph represents a different simulation. The BH had an initial NK of 400 km/s. The simulation corresponds to the pre-supernova stellar model of 21$M_\odot$.

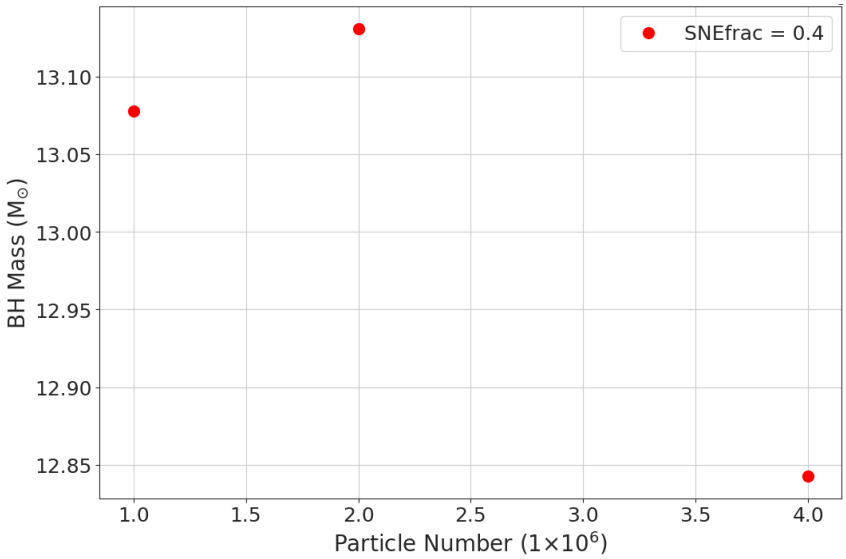

Figure A.2: Final mass of the BH after accretion, as a function of the number of SPH particles. Each point in the graph represents a different simulation. The BH had an initial NK of 400 km/s. The simulation corresponds to the pre-supernova stellar model of $21M_\odot$.

A.2 Properties of the Black Hole after accretion

The results are presented in the same order as in the Section 4.1 for the $28M_\odot$ star.

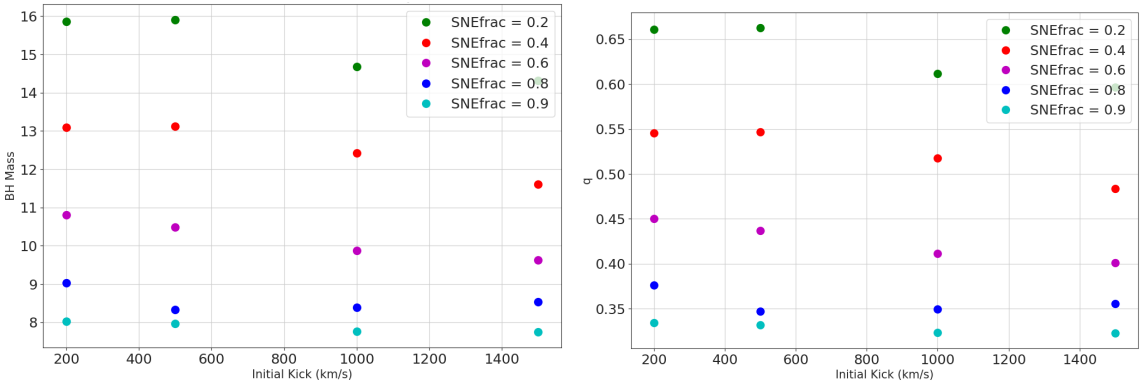

Figure A.3: **Left:** Final mass of the BH after accretion vs the initial NK. **Right:** Final mass fraction of the binary system after accretion, assuming a secondary star of $24M_\odot$.

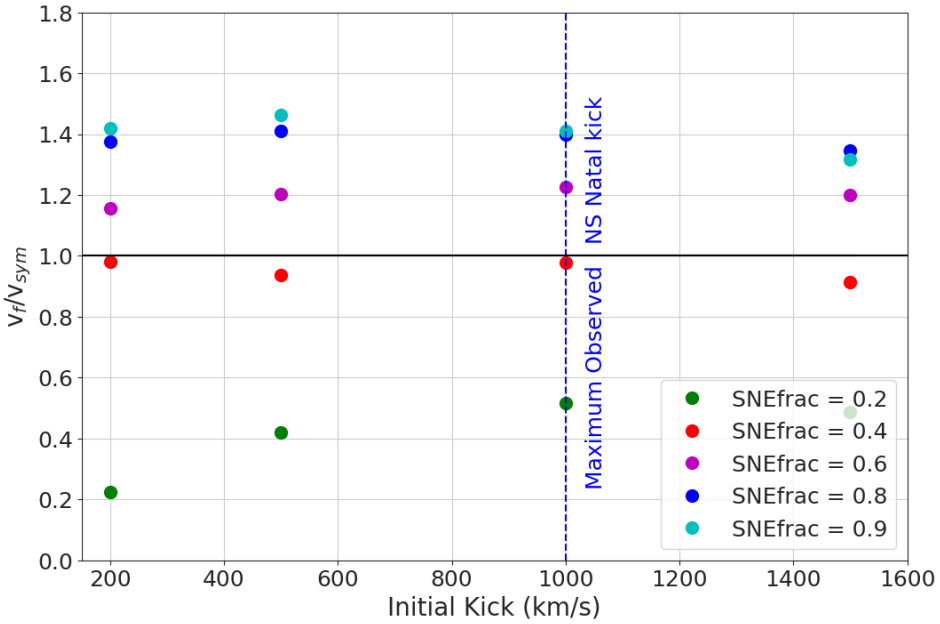

Figure A.4: Fraction between final BH speed and speed expected from accretion vs initial BH speed, for different explosion energies, with $N_{SPH} = 10^6$. The simulation corresponds to the pre-supernova stellar model of $21M_\odot$.

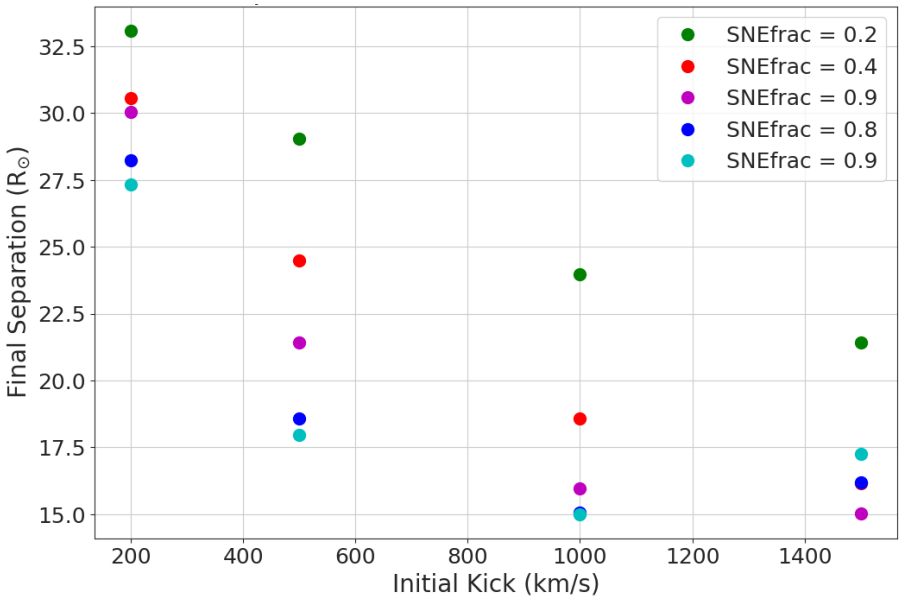

Figure A.5: Calculated final separation, assuming instantaneous mass loss, vs initial BH speed, for different explosion energies, with $N_{SPH} = 10^6$. The simulation corresponds to the pre-supernova stellar model of $21M_\odot$. The calculations are based on Brandt & Podsialowski 1995, assuming a secondary star of $24M_\odot$ and an initial separation of $40R_\odot$. [9]

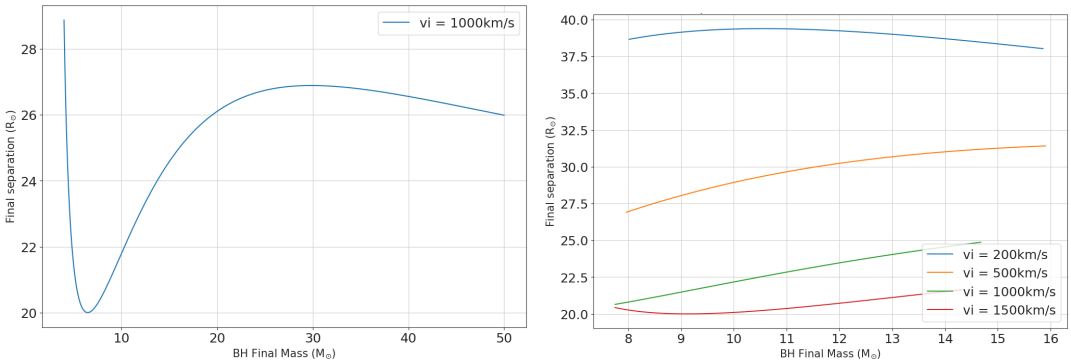

Figure A.6: **Left:** Final separation as a function of the final mass of the BH, assuming spherically symmetric accretion and an initial kick of 1000km/s. **Right:** Final separations as a function of the final mass of the BH, assuming spherically symmetric accretion. The calculations for both figures are based on Brandt & Podsialowski 1995, assuming a secondary star of $24M_{\odot}$ and an initial separation of $40R_{\odot}$. [9]

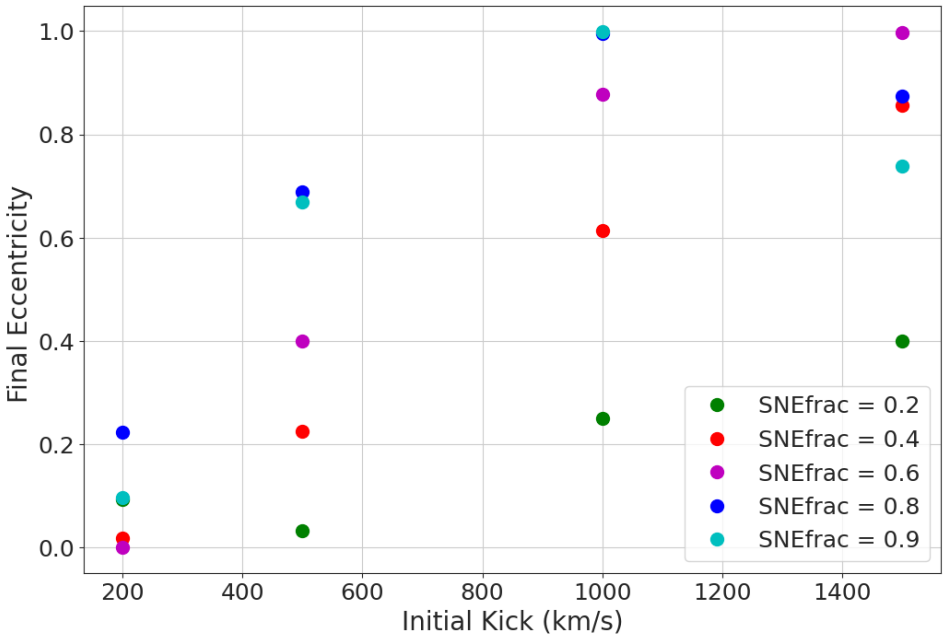

Figure A.7: Calculated final eccentricity, assuming instantaneous mass loss, vs initial BH speed, for different explosion energies, with $N_{SPH} = 10^6$. The simulation corresponds to the pre-supernova stellar model of $21M_{\odot}$. The calculations are based on Brandt & Podsialowski 1995, assuming a secondary star of $24M_{\odot}$. [9]

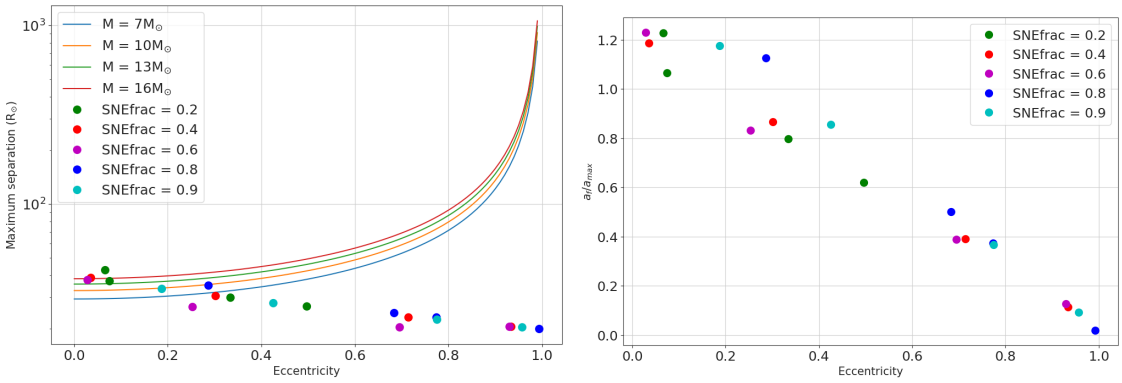

Figure A.8: **Left:** Maximum separation allowed for a binary system to be observed through GWs, as a function of the eccentricity after the NK. The solid lines represents how the maximum separation changes with eccentricity for different masses. The dots represent the final separation in the simulations. **Right:** Fraction between the final separation and the maximum separation allowed for a binary system to be observed through GWs, as a function of the Final eccentricity of the orbit. The calculations for the final separation and eccentricity are based on Brandt & Podsialowski 1995, assuming a secondary star of $24M_{\odot}$ and an initial separation of $40R_{\odot}$. [9]. The maximum separation is calculated based on the review of Postnov & Yungelson 2014 [26].

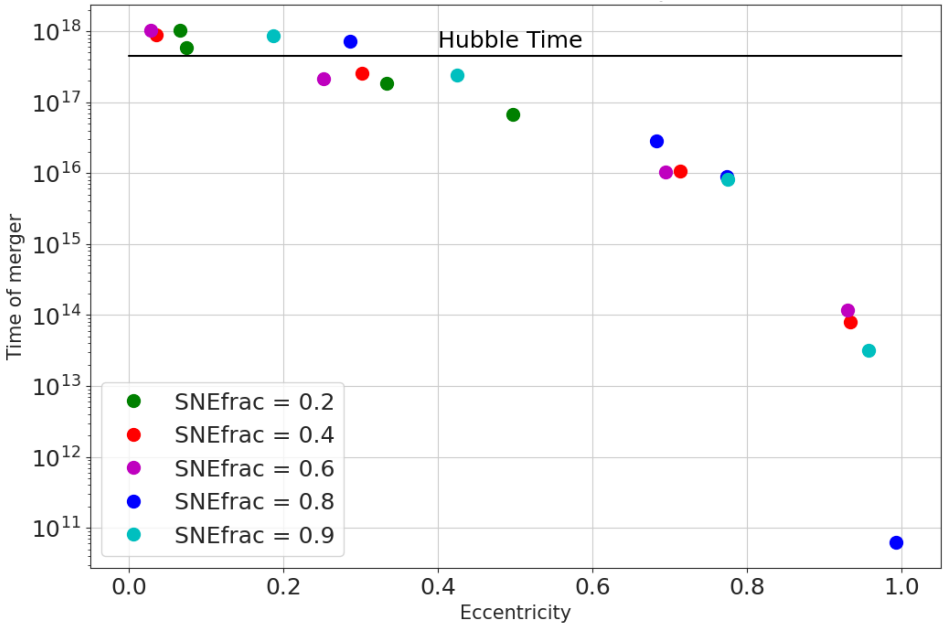

Figure A.9: Calculated time of merger for the BBH, vs eccentricity, for different explosion energies, with $N_{SPH} = 10^6$. The solid black line corresponds to the Hubble time.

Bibliography

[1] Abbott, R. et al. (LIGO Scientific Collaboration and Virgo Collaboration) GWTC-2: Compact Binary Coalescences Observed by LIGO and Virgo during the First Half of the Third Observing Run, Physical Review X, X 11, 021053, 2021. https://doi.org/10.1103/PhysRevX.11.021053

[2] Abbott, R. et al. (LIGO Scientific Collaboration and Virgo Collaboration) Properties of the Binary Black Hole Merger GW150914, Physical Review Letters, 116, 241102, 2016. https://doi.org/10.1103/PhysRevLett.116.241102

[3] Batta, A. Colapso y Acreción en Núcleos Estelares con Rotación, tesis doctoral, Universidad Nacional Autónoma de México, 2014.

[4] Batta, A., Ramirez-Ruiz, E., Fryer, C. The Formation of Rapidly Rotating Black Holes in High-mass X-Ray Binaries, Astrophysical Journal, 15, 846, 2017. https://doi.org/10.3847/2041-8213/aa8506

[5] Bavera, S. et al. The origin of spin in binary black holes: Predicting the distributions of the main observables of Advanced LIGO, Astronomy & Astrophysics, A97, 635, 2020. https://doi.org/10.1051/0004-6361/201936204

[6] Belczynski, K. et al. The first gravitational-wave source from the isolated evolution of two stars in the 40-100 solar mass range, Nature, 534, 512–515 , 2016. https://doi.org/10.1038/nature18322

[7] Belczynski, K. et al. The effect of metallicity on the detection prospects for gravitational waves, The Astrophysical Journal Letters, 715, L138 , 2010. https://doi.org/10.1088/2041-8205/715/2/L138

[8] Benacquista, M., Downing, J. Relativistic Binaries in Globular Clusters, Living Reviews in Relativity, 16, 4 , 2013.
https://doi.org/10.12942/lrr-2013-4

[9] Brandt, N., Podsialowski, P. The effects of high-velocity supernova kicks on the orbital properties and sky distributions of neutron-star binaries, Monthly Notices of the Royal Astronomical Society, 2, 274, 1995.
https://doi.org/10.1093/mnras/274.2.461

[10] Coleman, M. Implications of the gravitational wave event GW150914, General Relativity and Gravitation volume, 48, 95, 2016.
https://doi.org/10.1007/s10714-016-2088-4

[11] Górski, K. et al. HEALPix: A Framework for High-Resolution Discretization and Fast Analysis of Data Distributed on the Sphere, Astrophysical Journal, 622, 759, 2005.
https://doi.org/10.1086/427976

[12] Hall, P., Tout, C. Core radii and common-envelope evolution, Monthly Notices of the Royal Astronomical Societ, 444, 4, 2014.
https://doi.org/10.1093/mnras/stu1678

[13] Hilditch, R. W. An Introduction to Close Binary Stars, Cambridge University Press, New York, 2001.

[14] Hills, J. The effects of sudden mass loss and a random kick velocity produced in a supernova explosion on the dynamics of a binary star of arbitrary orbital eccentricity. Applications to X-ray binaries and to the binarypulsars, Astrophysical Journal, 267, 322-333, 1983.
https://doi.org/10.1086/160871

[15] Igoshev, A. et al. Combined analysis of neutron star natal kicks using proper motions and parallax measurements for radio pulsars and Be X-ray binaries, Monthly Notices of the Royal Astronomical Society, 508, 3, 2021.
https://doi.org/10.1086/160871

[16] Ivanova, N. et al. Formation of Black Hole X-Ray Binaries in Globular Clusters, The Astrophysical Journal, 717, 2, 2010.
https://doi.org/10.1093/mnras/stab2734

[17] Ivanova, N. et al. Common envelope evolution: where we stand and how we can move forward, The Astronomy and Astrophysics Review, 21, 59, 2013.
https://doi.org/10.1007/s00159-013-0059-2

[18] Janka, H. Natal kicks of stellar mass black holes by asymmetric mass ejection in fallback supernovae, Monthly Notices of the Royal Astronomical Society 2, 434, 2013.
https://doi.org/10.1093/mnras/stt1106

[19] Janka, H. Neutron Star Kicks by the Gravitational Tug-boat Mechanism in Asymmetric Supernova Explosions: Progenitor and Explosion Dependence, The Astrophysical Journal, 84, 837, 2017.
https://doi.org/10.3847/1538-4357/aa618e

[20] LIGO Scientifc and VIRGO Collaborations The basic physics of the binary black hole merger GW150914, Annalen der Physik, 1-2, 529 2017.
https://doi.org/10.1002/andp.201600209

[21] Mandel, I. Estimates of black hole natal kick velocities from observations of low-mass X-ray binaries, Monthly Notices of the Royal Astronomical Society, 1, 456, 2016.
https://doi.org/10.1093/mnras/stv2733

[22] Mandel, I., Müller, B. Simple recipes for compact remnant masses and natal kicks, Monthly Notices of the Royal Astronomical Society, 3, 499, 2020.
https://doi.org/10.1093/mnras/staa3043

[23] Mapelli, M. Formation Channels of Single and Binary Stellar-Mass Black Holes, In: Bambi, C., Katsanevas, S., Kokkotas, K.D. (eds) Handbook of Gravitational Wave Astronomy., Springer, Singapore, 2021.
https://doi.org/10.1007/978-981-15-4702-7_16-1

[24] Matzner C., McKee C., The Expulsion of Stellar Envelopes in Core-Collapse Supernovae, American Astronomical Society, 1, 510, 1999.
https://doi.org/10.1086/306571

[25] Miller, C. Implications of the gravitational wave event GW150914, General Relativity and Gravitation, 48, 95, 2016.
https://doi.org/10.1007/s10714-016-2088-4

[26] Postnov, K., Yungelson, L. The Evolution of Compact Binary Star Systems, Living Reviews in Relativity, 3, 17, 2014.
https://doi.org/10.12942/lrr-2014-3

[27] Price, D. Smoothed particle hydrodynamics and magnetohydrodynamics, Journal of Computational Physics, 231, 759-794, 2012.
https://doi.org/10.1016/j.jcp.2010.12.011

[28] Price, D. Smoothed Particle Hydrodynamics: Things I wish my mother taught me, Advances in computational astrophysics: methods, tools, and outcome. (Proceedings), 453, 2011.
https://doi.org/10.48550/arXiv.1111.1259

[29] Qin, Y. et al. The spin of the second-born black hole in coalescing binary black holes, Astronomy & Astrophysics, A28, 616, 2018.
https://doi.org/10.1051/0004-6361/201832839

[30] Repetto, S., Davies, M., Sigurdsson, S. Investigating stellar-mass black hole kicks, Monthly Notices of the Royal Astronomical Society, 4, 425, 2012.
https://doi.org/10.1111/j.1365-2966.2012.21549.x

[31] Rodriguez, C. et al. Illuminating Black Hole Binary Formation Channels with Spins in Advanced LIGO, Astrophysical Journal, 1, 832, 2016.
https://doi.org/10.3847/2041-8205/832/1/L2

[32] Rodriguez, C. et al. Post-Newtonian Dynamics in Dense Star Clusters: Highly Eccentric, Highly Spinning, and Repeated Binary Black Hole Mergers, Physical Review Letters, 120, 15, 2018.
https://doi.org/10.1103/PhysRevLett.120.151101

[33] Sana, H. et al., Binary Interaction Dominates the Evolution of Massive Stars, SCIENCE, 337, 6093, 2012.
https://doi.org/10.1126/science.1223344

[34] Schrøder, S., Evolutionary Scenarios of Binaries Hosting Supernova Progenitors, University of Copenhagen, Niels Bohr Institute, Phd thesis, 2016.

[35] Schrøder, S., Batta, A., Ramirez-Ruiz, E. Black Hole Formation in Fallback Supernova and the Spins of LIGO Sources, The Astrophysical Journal, 3, 862, 2018.
https://doi.org/10.3847/2041-8213/aacf8d

[36] Springel, V. The cosmological simulation code GADGET-2, Monthly Notices of the Royal Astronomical Society, 364, 4, 2005.
https://doi.org/10.1111/j.1365-2966.2005.09655.x

[37] Springel, V.; Yoshida, N.; White, S. GADGET: a code for collisionless and gasdynamical cosmological simulations, New Astronomy, 6, 2, 2001.
https://doi.org/10.1016/S1384-1076(01)00042-2

[38] Verbunt, F.; Igoshev, A.; Cator, E. The observed velocity distribution of young pulsars, Astronomy & Astrophysics, 608, A57, 2017.
https://doi.org/10.1051/0004-6361/201731518

[39] Vigna-Gomez, A. et al. Fallback Supernova Assembly of Heavy Binary Neutron Stars and Light Black Hole– Neutron Star Pairs and the Common Stellar Ancestry of GW190425 and GW200115, Astrophysical Journal, 17, 920, 2021.
https://doi.org/10.3847/2041-8213/ac2903

[40] Woosley, S.; Heger, A. The Progenitor Stars of Gamma-Ray Bursts, Astrophysical Journal, 637, 914, 2006.
https://doi.org/10.1086/498500